

# Isospin Asymmetry in Nuclei and Neutron Stars

A.W. Steiner,<sup>1,2</sup> M. Prakash,<sup>3</sup> J.M. Lattimer,<sup>3</sup> and P.J. Ellis<sup>1</sup>

<sup>1</sup>*School of Physics and Astronomy, University of Minnesota, Minneapolis, MN 55455-0112*

<sup>2</sup>*Theoretical Division, Los Alamos National Laboratory, Los Alamos, NM 87545*

<sup>3</sup>*Department of Physics and Astronomy, SUNY at Stony Brook, Stony Brook, New York 11794-3800*

The roles of isospin asymmetry in nuclei and neutron stars are investigated using a range of potential and field-theoretical models of nucleonic matter. The parameters of these models are fixed by fitting the properties of homogeneous bulk matter and closed-shell nuclei. We discuss and unravel the causes of correlations among the neutron skin thickness in heavy nuclei, the pressure of beta-equilibrated matter at a density of  $0.1 \text{ fm}^{-3}$ , the derivative of the nuclear symmetry energy at the same density and the radii of moderate mass neutron stars. Constraints on the symmetry properties of nuclear matter from the binding energies of nuclei are examined. The extent to which forthcoming neutron skin measurements will further delimit the symmetry properties is investigated. The impact of symmetry energy constraints for the mass and moment of inertia contained within neutron star crusts and the threshold density for the nucleon direct Urca process, all of which are potentially measurable, is explored. We also comment on the minimum neutron star radius, assuming that only nucleonic matter exists within the star.

PACS numbers: 26.60.+c, 21.10.-k, 97.60.Jd, 21.10.Gv, 21.65.+f

Keywords: Nuclei; Neutron Stars; Isospin Asymmetry

## Contents

<b>I. INTRODUCTION</b>	3
<b>II. EFFECTIVE THEORIES</b>	5
A. Potential Models	5
B. Field Theoretical Models	7
C. The EOS of Akmal-Pandharipande-Ravenhall	8
<b>III. SEMI-INFINITE NUCLEONIC MATTER</b>	10
A. Variational Approach	11
1. Potential Models	13
2. Field Theoretical Models	15
B. Relationship to the Liquid Droplet Model of Nuclei	17
1. “ $\mu_n$ ” Approach	18
2. “ $\mu_\alpha$ ” Approach	20
<b>IV. RESULTS</b>	21
A. Selection of Models and Their Parameters	21
Results for the EOS of APR	22
B. Semi-infinite matter and finite nuclei	25
C. Correlations and Their Origins	26
1. Nuclear masses and the correlation between $S_s$ and $S_v$	26
2. The neutron skin thickness versus the pressure of subnuclear neutron-star matter	30
Implications for neutrino emission from neutron stars	33
Implications for the crustal fraction of the moment of inertia	34
3. The neutron star radius versus the pressure of supranuclear neutron-star matter	36
Sizes of neutron star radii in potential and field-theoretical models	37
4. The neutron skin thickness versus the neutron star radius	38
<b>V. OTHER RELATED CORRELATIONS</b>	39
A. Giant Dipole Resonances	39
B. Heavy-Ion Collisions	41
1. Multi-fragmentation	41
2. Collective Flow	42
<b>VI. DISCUSSION AND CONCLUSIONS</b>	42
<b>ACKNOWLEDGMENTS</b>	44
<b>A. Model properties</b>	45
<b>B. Coupling strengths of models SR2, es25, es30, and es35</b>	46
<b>References</b>	47

## I. INTRODUCTION

Strongly interacting matter in which more neutrons than protons exist is encountered in both heavy nuclei and neutron stars. In stable nuclei the net asymmetry  $I = (N - Z)/(N + Z)$  ranges up to about 0.24, but the neutron-to-proton asymmetry,  $\delta = (n_n - n_p)/n$  where  $n_n$  and  $n_p$  are the number densities of neutrons and protons and  $n = n_n + n_p$ , approaches unity in the nuclear surface. In the future, rare-isotope accelerator experiments will extend the range of  $I$  to values well in excess of 0.2. In contrast,  $I$  could be as large as 0.95 in the interiors of neutron stars. The physical properties of nuclei, such as their masses, neutron and proton density distributions (including their mean radii), collective excitations, fission properties, matter and momentum flows in high energy heavy-ion collisions, etc. all depend on the isospin structure of the strong interactions between nucleons (i.e.,  $nn$  and  $pp$  interactions versus  $np$  interactions). The energetics associated with the  $n - p$  asymmetry can be characterized by the so-called symmetry energy,  $E_{sym}$ , which is the leading coefficient of an expansion of the total energy with respect to asymmetry:  $E(n, \delta) \approx E_0(n) + E_{sym}\delta^2 \dots$ . The energy  $\hat{\mu} = \mu_n - \mu_p \cong 4E_{sym}\delta$ , where  $\mu_n$  and  $\mu_p$  are the neutron and proton chemical potentials, respectively, is crucial in determining reaction rates involving electrons and neutrinos, particle abundances, etc., in astrophysical contexts such as supernova dynamics, proto-neutron star evolution, the  $r$ -process, the long-term cooling of neutron stars, and the structure of cold-catalyzed neutron stars (i.e. their masses, radii and crustal extent), etc. The pervasive role of the isospin dependence of strong interactions in nuclear processes in the laboratory and the cosmos is sketched in Fig. 1. In this work some of these connections will be discussed.

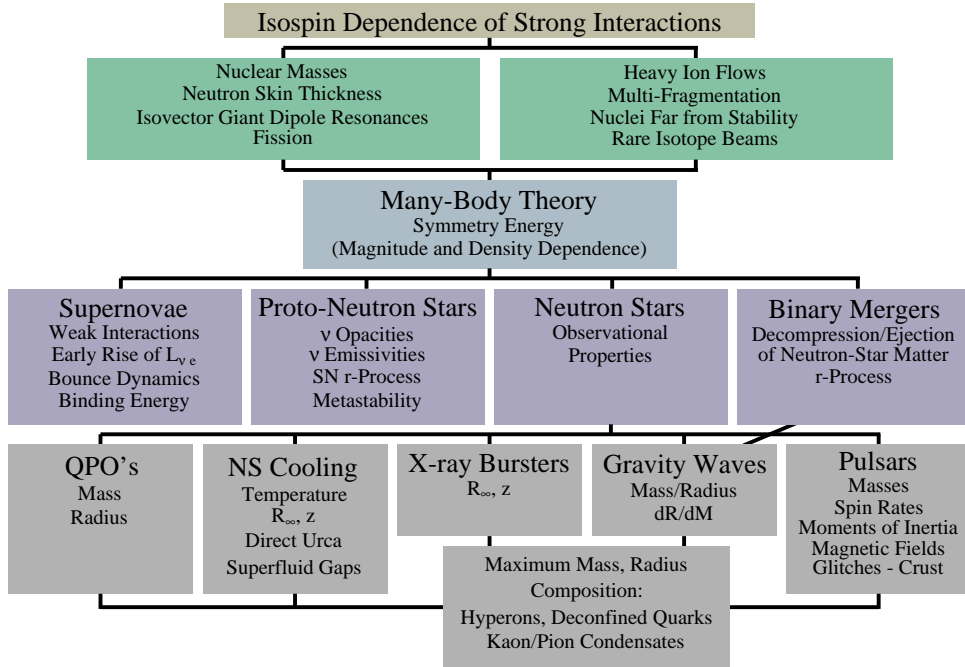


FIG. 1: The multifaceted influence of the nuclear symmetry energy.

Recently, several empirical relationships have been discovered that underscore the role of isospin interactions in nuclei and neutron stars. These include correlations between:

1. *The neutron star radius  $R$  and the pressure  $P$  of neutron-star matter.* Lattimer and Prakash [1, 2] found that the quantity  $RP^{-1/4}$  is approximately constant, for a given neutron star

mass, for a wide variety of equations of state when the pressure  $P$  of beta-equilibrated neutron-star matter is evaluated at a density in the range  $n_0$  to  $2n_0$ , where  $n_0$  denotes equilibrium nuclear matter density. Since the pressure of nearly pure neutron matter (a good approximation to neutron star matter) near  $n_0$  is approximately given by  $n^2 \partial E_{sym} / \partial n$ , the density dependence of the symmetry energy just above  $n_0$  will be a critical factor in determining the neutron star radius.

2. *The neutron skin thickness in nuclei and the pressure of pure neutron matter at sub-nuclear density:* Typel and Brown [3, 4] have noted that model calculations of the difference between neutron and proton rms radii  $\delta R = \langle r_n^2 \rangle^{1/2} - \langle r_p^2 \rangle^{1/2}$  are linearly correlated with the pressure of pure neutron matter at a density below  $n_0$  characteristic of the mean density in the nuclear surface (e.g.,  $0.1 \text{ fm}^{-3}$ ). The density dependence of the symmetry energy controls  $\delta R$  (we will call this the neutron skin thickness) in a heavy, neutron-rich nucleus. Explicitly,  $\delta R$  is proportional to a specific average of  $[1 - E_{sym}(n_0)/E_{sym}(n)]$  in the nuclear surface, see Refs. [5, 6] and Eq. (102) below.
3. *The neutron skin thickness in nuclei and the neutron star radius:* Horowitz and Piekarewicz [7] have pointed out that models that yield smaller neutron skins in heavy nuclei tend to yield smaller neutron star radii. These authors, along with others [8, 9], have also pointed out the need for an accurate measurement of the neutron skin.

Unlike proton distributions, neutron distributions in nuclei have remained uncertain to this date. Recent studies of neutron densities from a global analysis of medium-energy proton scattering on  $^{208}\text{Pb}$  indicate that  $0.07 < \delta R < 0.16 \text{ fm}$  [10]. Related information is also available from an analysis of antiprotonic atom data that gives  $\delta R = 0.15 \pm 0.02 \text{ fm}$  [11]. In the latter work, nucleon density distributions are parameterized by Fermi functions and it is found that the half-density radii for neutrons and protons in heavy nuclei are the same, but the diffuseness parameter for the neutrons is larger than that for the protons. Skin thicknesses as large as  $0.2 \text{ fm}$  were obtained in earlier analyses; see the discussion of Karataglidis et al. [12]. Since these studies involve strongly interacting probes, even to this date the value of  $\delta R$  for a nucleus such as  $^{208}\text{Pb}$  is not accurately known. This situation should improve as it is expected that the neutron rms radius will be determined to about 1% accuracy by measuring the parity-violating electroweak asymmetry in the elastic scattering of polarized electrons from  $^{208}\text{Pb}$  [8], an experiment planned at the Jefferson Laboratory [9].

A common theme in the evaluation of the neutron skin thickness and the pressure of neutron star matter below and above the saturation density  $n_0$  is the density dependence of the isospin asymmetric part of the nuclear interaction. To highlight this dependence, we examine theoretical predictions of  $\delta R$  and the neutron star radius for an extensive set of potential and field-theoretical models. For the former we employ Skyrme-like potential model interactions, including a parameterization [13] of the microscopic calculations of Akmal and Pandharipande [14]. For the latter field-theoretical models we use Walecka-type models [15] in which nucleons interact through the exchange of  $\sigma$ ,  $\omega$  and  $\rho$  mesons augmented with additional mesonic couplings (see, for example, Horowitz and Piekarewicz [7]) to better describe the properties of nuclei and explore the properties of neutron stars. In order to provide baseline calculations, our investigations will be restricted to the case in which the high density phase of neutron stars contains nucleons (and enough electrons and muons to neutralize the matter) only.

Our goals in this work are to identify the causes of the correlations mentioned above through a semi-analytic analysis of detailed calculations and to uncover other possible correlations. Toward these goals, we investigate an assortment of potential and field-theoretical models that cover a range of symmetry properties and incompressibilities, but which are constrained by the empirical

properties of isospin symmetric and asymmetric nuclear matter, and the binding energies and radii of closed shell nuclei. The properties of nuclei are investigated through Hartree-Fock-Bogoliubov calculations for potential models and Hartree calculations for field theoretical models. In both categories, our calculations include models that match the Akmal and Pandharipande [14] equation of state (EOS) as results for nuclei with this model are not available in the literature. Additional insights are provided through analytical and numerical analyses of isospin asymmetric semi-infinite matter in the potential and field theoretical approaches. The results of these calculations are utilized in understanding several correlations in conjunction with inferences from nuclear masses. The neutron skin-pressure and neutron star radius-pressure correlations are reexamined to provide improved relations. Our calculations also provide an estimate of the smallest neutron star radii that ensue from these models.

The presentation is organized as follows. In Sec. II, the Hamiltonian (Lagrangian) densities of the potential (field-theoretical) models used in this work are described. The variational approach to determine the bulk and surface properties of isospin asymmetric semi-infinite nucleonic matter in these models is developed in Sec. III. This section also contains a discussion of how these properties enter in the liquid droplet model description of nuclei. Our results and discussion of the various correlations, and their origins are presented in Sec. IV. Section V contains a brief description of other related correlations. Discussion and conclusions are contained in Sec. VI. Appendix A lists the properties of the models used in this work. The coupling strengths of some newly-constructed models are given in Appendix B.

## II. EFFECTIVE THEORIES

In both potential and field-theoretical model descriptions of many-body systems, the Hohenberg-Kohn-Sham theorem [16, 17] allows the total Hamiltonian density to be expressed in terms of the local particle number and kinetic energy densities of the various species. This simplification is of great utility in the study of both heavy nuclei and infinite matter since microscopic calculations, such as variational/Monte Carlo studies starting from a Hamiltonian constructed on the basis of nucleon-nucleon and many-nucleon interactions, are computer intensive and are only beginning to be undertaken for heavy nuclei (for a review of such studies on light nuclei, see Ref. [18]). In practice, the strengths of the various interactions in the density functional approach are determined by appealing to available data. In the following, we consider both potential and field theoretical approaches so that distinguishing traits between these approaches can be identified.

### A. Potential Models

A commonly employed non-relativistic effective Hamiltonian density stems from Skyrme's work [19] in which finite-range forces between nucleons were approximated by effective zero-range forces. For low relative momenta (i.e., with  $s$ - and  $p$ -wave interactions only), the resulting Hamiltonian density takes the form [20]

$$\mathcal{H} = \mathcal{H}_B + \frac{1}{2} \left[ Q_{nn} (\vec{\nabla} n_n)^2 + 2Q_{np} \vec{\nabla} n_n \cdot \vec{\nabla} n_p + Q_{pp} (\vec{\nabla} n_p)^2 \right] + \mathcal{H}_C + \mathcal{H}_J, \quad (1)$$

where the term associated with spatially homogeneous bulk matter is of the form

$$\begin{aligned} \mathcal{H}_B = & \frac{\hbar^2}{2m_n} \tau_n + \frac{\hbar^2}{2m_p} \tau_p + n (\tau_n + \tau_p) \left[ \frac{t_1}{4} \left( 1 + \frac{x_1}{2} \right) + \frac{t_2}{4} \left( 1 + \frac{x_2}{2} \right) \right] \\ & + (\tau_n n_n + \tau_p n_p) \left[ \frac{t_2}{4} \left( \frac{1}{2} + x_2 \right) - \frac{t_1}{4} \left( \frac{1}{2} + x_1 \right) \right] \end{aligned}$$

$$\begin{aligned}
& + \frac{t_0}{2} \left[ \left( 1 + \frac{x_0}{2} \right) n^2 - \left( \frac{1}{2} + x_0 \right) (n_n^2 + n_p^2) \right] \\
& + \frac{t_3}{12} \left[ \left( 1 + \frac{x_3}{2} \right) n^2 - \left( \frac{1}{2} + x_3 \right) (n_n^2 + n_p^2) \right] n^\epsilon. \tag{2}
\end{aligned}$$

Above,  $m_n$  and  $m_p$  are the masses of the neutron and the proton (these will often be taken to be equal and then denoted by  $M$ ),  $n_n$  and  $n_p$  are the number densities of neutrons and protons, and  $t_0, t_1, t_2, t_3, x_0, x_1, x_2, x_3$ , and  $\epsilon$  are parameters that give the strengths of the various potential interactions. We recall that total baryon density is  $n = n_n + n_p$ . The first two terms represent the kinetic energy densities for the neutron and the proton respectively, the sixth term is the density-dependent form of the zero-range multi-body force, and the remaining terms constitute the  $s$ - and  $p$ -wave parts of the two-body interaction.

The coefficients  $Q$  associated with the spatially varying part of the Hamiltonian density in Eq. (1) are given by

$$Q_{nn} = Q_{pp} = \frac{3}{16} [t_1(1-x_1) - t_2(1+x_2)], \tag{3}$$

$$Q_{np} = Q_{pn} = \frac{1}{8} \left[ 3t_1 \left( 1 + \frac{x_1}{2} \right) - t_2 \left( 1 + \frac{x_2}{2} \right) \right]. \tag{4}$$

Note that for a Skyrme-type force, the  $Q$ 's are constants. However, in general, it is possible for the  $Q$ 's to be density-dependent functions. Also note that, for Skyrme-type forces,  $Q_{nn} = Q_{pp}$ , but this does not have to be true in general. Generally, we have  $Q_{np} = Q_{pn}$  however.

The term  $\mathcal{H}_C$  in Eq. (1) arising from the Coulomb interaction is

$$\mathcal{H}_C(\vec{r}) = \frac{e^2 n_p(\vec{r})}{2} \int d^3 r' \frac{n_p(\vec{r}')}{|\vec{r} - \vec{r}'|} - \frac{3e^2}{4} \left( \frac{3}{\pi} \right)^{1/3} n_p(\vec{r})^{4/3}, \tag{5}$$

where  $e$  denotes the proton's electric charge and the second term is an exchange correction [21]. The term  $\mathcal{H}_J$  arising from the spin orbit interaction is

$$\begin{aligned}
\mathcal{H}_J = & -\frac{W_0}{2} \left( n_n \vec{\nabla} \cdot \vec{J}_n + n_p \vec{\nabla} \cdot \vec{J}_p + n \vec{\nabla} \cdot \vec{J} \right) \\
& + \frac{t_1}{16} \left( \vec{J}_n^2 + \vec{J}_p^2 - x_1 \vec{J}^2 \right) - \frac{t_2}{16} \left( \vec{J}_n^2 + \vec{J}_p^2 + x_2 \vec{J}^2 \right), \tag{6}
\end{aligned}$$

where the neutron spin-orbit density  $\vec{J}_n = \sum_i^{neutron} \psi_i^\dagger \vec{\sigma} \times \vec{\nabla} \psi_i$ , similarly for protons and  $\vec{J} = \vec{J}_n + \vec{J}_p$ .

The use of Skyrme's effective interactions has successfully reproduced many of the global properties of nuclei including binding energies, charge radii, etc. [22]. The properties of bulk symmetric nuclear matter at the saturation density  $n_0$ , can be expressed directly in terms of  $n_0$ , and the model parameters. Explicitly, the energy per nucleon  $E/A$ , the effective mass  $M^*$ , the pressure per particle  $P/n$  and the compressibility  $K$  are given by

$$\frac{E}{A} = C n_0^{2/3} (1 + \beta n_0) + \frac{3t_0}{8} n_0 + \frac{t_3}{16} n_0^{\epsilon+1}, \tag{7}$$

$$C = \frac{3\hbar^2}{10M} \left( \frac{3\pi^2}{2} \right)^{2/3}; \quad \beta = \frac{M}{2\hbar^2} \left[ \frac{1}{4} (3t_1 + 5t_2) + t_2 x_2 \right], \tag{8}$$

$$M^*/M = (1 + \beta n_0)^{-1}, \tag{9}$$

$$\frac{P(n_0)}{n_0} = 0 = \frac{2}{3} C n_0^{2/3} \left( 1 + \frac{5}{2} \beta n_0 \right) + \frac{3}{8} t_0 n_0 + \frac{t_3}{16} (\epsilon + 1) n_0^{\epsilon+1}, \tag{10}$$

$$K = 9n^2 \frac{\partial^2 E/A}{\partial n^2} \Big|_{n=n_0} = -2C n_0^{2/3} + 10C\beta n_0^{5/3} + \frac{9t_3}{16} \epsilon (\epsilon + 1) n_0^{\epsilon+1}. \tag{11}$$

The symmetry energy of bulk matter,  $E_{sym}$ , is

$$E_{sym}(n) = \frac{n^2}{2} \frac{\partial^2 E/A}{\partial \alpha^2} \Big|_{\alpha=0} = \frac{5}{9} C n^{2/3} + \frac{10CM}{3\hbar^2} \left[ \frac{t_2}{6} \left( 1 + \frac{5}{4} x_2 \right) - \frac{1}{8} t_1 x_1 \right] n^{5/3} - \frac{t_3}{24} \left( \frac{1}{2} + x_3 \right) n^{\epsilon+1} - \frac{t_0}{4} \left( \frac{1}{2} + x_0 \right) n, \quad (12)$$

where the isospin asymmetry density is denoted by  $\alpha = n_n - n_p$ . The volume symmetry energy of equilibrium nuclear matter  $E_{sym}(n_0)$  will be denoted  $S_v$ . We note that the symmetry energy asymptotically decreases at large densities if  $\epsilon > 2/3$  or  $t_1 x_1 > t_2(4 + 5x_2)/3$ . (This poor high-density behavior can be remedied [23].) For models in which the symmetry energy monotonically increases with density, the negative sign of the multi-body term involving  $t_3$  generally results in neutron star radii which are smaller than in field-theoretical models (see Sec. IV C 3).

## B. Field Theoretical Models

The structure of nuclei and the properties of high-density nucleonic matter have also been studied utilizing the mean field approximation to a Walecka-type Lagrangian that couples nucleons to scalar ( $\sigma$ ), vector ( $\omega_\mu$ ), and vector-isovector ( $\vec{\rho}_\mu$ ) mesons and photons ( $A_\mu$ ) [24]. The Lagrangian, supplemented by non-linear interactions, is

$$\mathcal{L} = \bar{\Psi} \left[ i\partial\!\!\!/ - g_\omega \psi - \frac{1}{2} g_\rho \vec{\rho} \cdot \vec{\tau} - M + g_\sigma \sigma - \frac{1}{2} e(1 + \tau_3) \mathcal{A} \right] \Psi + \frac{1}{2} (\partial_\mu \sigma)^2 - V(\sigma) - \frac{1}{4} f_{\mu\nu} f^{\mu\nu} + \frac{1}{2} m_\omega^2 \omega^\mu \omega_\mu - \frac{1}{4} \vec{B}_{\mu\nu} \cdot \vec{B}^{\mu\nu} + \frac{1}{2} m_\rho^2 \vec{\rho}^\mu \cdot \vec{\rho}_\mu - \frac{1}{4} F_{\mu\nu} F^{\mu\nu} + \frac{\zeta}{24} g_\omega^4 (\omega^\mu \omega_\mu)^2 + \frac{\xi}{24} g_\rho^4 (\vec{\rho}^\mu \cdot \vec{\rho}_\mu)^2 + g_\rho^2 f(\sigma, \omega_\mu \omega^\mu) \vec{\rho}^\mu \cdot \vec{\rho}_\mu, \quad (13)$$

where  $\vec{\tau}$  are the SU(2) isospin matrices,  $f_{\mu\nu} = \partial_\mu \omega_\nu - \partial_\nu \omega_\mu$ ,  $\vec{B}_{\mu\nu} = \partial_\mu \vec{\rho}_\nu - \partial_\nu \vec{\rho}_\mu$ ,  $F_{\mu\nu} = \partial_\mu A_\nu - \partial_\nu A_\mu$  and the scalar meson potential

$$V(\sigma) = \frac{1}{2} m_\sigma^2 \sigma^2 + \frac{\kappa}{6} (g_\sigma \sigma)^3 + \frac{\lambda}{24} (g_\sigma \sigma)^4. \quad (14)$$

In Sec. IV, we discuss the choice of the couplings  $g_\sigma$ ,  $g_\omega$ ,  $g_\rho$ ,  $\kappa$  (dimensionful) and  $\lambda$ , as well as  $\zeta$  and  $\xi$  that allow the high-density behavior of the equation of state to be varied. The first five of these are constrained to reproduce the properties of equilibrium nuclear matter and the empirical symmetry energy. Horowitz and Piekarewicz [7] have extended the non-linear Walecka model by adding  $\sigma^2 \vec{\rho}^\mu \cdot \vec{\rho}_\mu$  and  $\omega_\mu \omega^\mu \vec{\rho}^\mu \cdot \vec{\rho}_\mu$  terms to the Lagrangian so as to modify the density dependence of the symmetry energy at supranuclear densities (in the absence of this coupling the dependence is linear at large densities). In order to provide additional freedom in varying the symmetry energy we have adopted a general function  $f$ , namely

$$f(\sigma, \omega_\mu \omega^\mu) = \sum_{i=1}^6 a_i \sigma^i + \sum_{j=1}^3 b_j (\omega_\mu \omega^\mu)^j. \quad (15)$$

Utilizing the mean field approximation with the Lagrangian (13), the binding energy per particle in symmetric matter at equilibrium is given by

$$B \equiv M - \frac{E}{A} = M - \frac{1}{n_0} \left[ V(\sigma_0) + \frac{1}{2} m_\omega \omega_0^2 + \frac{\zeta}{8} (g_\omega \omega_0)^4 + \frac{2}{\pi^2} \int_0^{k_F} dk k^2 \sqrt{k^2 + M^{*2}} \right], \quad (16)$$

where the Dirac effective mass is  $M^* = M - g_\sigma \sigma_0$ , and the Fermi momentum and energy of symmetric nuclear matter are, respectively,

$$k_F = \left( \frac{3\pi^2 n}{2} \right)^{1/3}, \quad E_F^* = \sqrt{k_F^2 + M^{*2}}. \quad (17)$$

The equilibrium pressure per particle is

$$\frac{P(n_0)}{n_0} = 0 = \frac{1}{n_0} \left[ -V(\sigma_0) + \frac{1}{2} m_\omega \omega_0^2 + \frac{\zeta}{24} (g_\omega \omega_0)^4 + \frac{2}{3\pi^2} \int_0^{k_F} dk \frac{k^4}{\sqrt{k^2 + M^{*2}}} \right], \quad (18)$$

and the compressibility at equilibrium is given by

$$K = 9n_0 \left[ \frac{m_\omega^2}{g_\omega^2} + \frac{\zeta}{2} (g_\omega \omega_0)^2 \right]^{-1} + 3 \frac{k_F^2}{E_F^*} - 9n_0 \left( \frac{M^*}{E_F^*} \right)^2 \left[ \left( \frac{1}{g_\sigma^2} \frac{\partial^2}{\partial \sigma_0^2} + \frac{3}{g_\sigma M^*} \frac{\partial}{\partial \sigma_0} \right) V(\sigma_0) - 3 \frac{n_0}{E_F^*} \right]^{-1}. \quad (19)$$

The symmetry energy of bulk matter is

$$E_{sym}(n) = \frac{k_F^2}{6E_F^*} + \frac{n}{8 \left( m_\rho^2/g_\rho^2 + 2f(\sigma_0, \omega_0^2) \right)}. \quad (20)$$

In the above equations, the subscript “0” denotes mean field values of  $\sigma$  and  $\omega$ . For the case  $f = 0$ , the symmetry energy in Eq. (20) varies linearly with the density at large densities. The presence of the function  $f$  permits variations in this density dependence.

### C. The EOS of Akmal-Pandharipande-Ravenhall

The results of the variational microscopic calculations of Akmal and Pandharipande [14], in which many-body and special relativistic corrections are progressively incorporated into prior models, have been parameterized by Akmal, Pandharipande and Ravenhall (hereafter APR) [13]. The bulk effective Hamiltonian density is

$$\mathcal{H}_{B,APR} = \left( \frac{\hbar^2}{2m} + (p_3 + (1-x)p_5) ne^{-p_4 n} \right) \tau_n + \left( \frac{\hbar^2}{2m} + (p_3 + xp_5) ne^{-p_4 n} \right) \tau_p + g_1 (1 - (1 - 2x)^2) + g_2 (1 - 2x)^2, \quad (21)$$

where  $\tau_n$  and  $\tau_p$  are the kinetic energy densities of the neutrons and protons, respectively and  $x = n_p/n$ . Contributions from potential interactions are contained in the functions  $g_1$  and  $g_2$  that have two different forms corresponding to the low density phase (LDP) and the high density phase (HDP) that contains a neutral pion condensed phase. Explicitly,

$$g_{1LDP} = -n^2 \left( p_1 + p_2 n + p_6 n^2 + (p_{10} + p_{11} n) e^{-p_9^2 n^2} \right), \quad (22)$$

$$g_{2LDP} = -n^2 \left( p_{12}/n + p_7 + p_8 n + p_{13} e^{-p_9^2 n^2} \right), \quad (23)$$

$$g_{1HDP} = g_{1LDP} - n^2 \left( p_{17} (n - p_{19}) + p_{21} (n - p_{19})^2 e^{p_{18}(n-p_{19})} \right), \quad (24)$$

$$g_{2HDP} = g_{2LDP} - n^2 \left( p_{15} (n - p_{20}) + p_{14} (n - p_{20})^2 e^{p_{16}(n-p_{20})} \right). \quad (25)$$

The numerical values of the various parameters  $p_i$  for the recommended “A18+ $\delta v$ +UIX\*” EOS,

TABLE I: Coupling strengths for the Hamiltonian density of APR in Eq. (21). The dimensions are such that the Hamiltonian density is in MeV fm<sup>-3</sup>.

$p_1$	$p_2$	$p_3$	$p_4$	$p_5$	$p_6$	$p_7$	$p_8$	$p_9$	$p_{10}$	$p_{11}$
337.2	-382	89.8	0.457	-59.0	-19.1	214.6	-384	6.4	69	-33
$p_{12}$	$p_{13}$	$p_{14}$	$p_{15}$	$p_{16}$	$p_{17}$	$p_{18}$	$p_{19}$	$p_{20}$	$p_{21}$	
0.35	0	0	287	-1.54	175.0	-1.45	0.32	0.195	0	

that incorporates three-nucleon interactions and relativistic boost corrections, are collected in Table I. For this EOS,  $n_0 = 0.16$  fm<sup>-3</sup>,  $E/A = -16$  MeV,  $M^*/M = 0.7$ ,  $K = 266$  MeV, and  $E_{sym}(n_0) = 32.6$  MeV.

For later use the Q's for the EOS of APR, calculated using the procedure detailed in Ref. [25], are

$$\begin{aligned} Q_{nn} &= \frac{1}{4}e^{-p_4 n} [-6p_5 - p_4(p_3 - 2p_5)(n_n + 2n_p)] , \\ Q_{pp} &= \frac{1}{4}e^{-p_4 n} [-6p_5 - p_4(p_3 - 2p_5)(n_p + 2n_n)] , \\ Q_{np} = Q_{pn} &= \frac{1}{8}e^{-p_4 n} [4(p_3 - 4p_5) - 3p_4(p_3 - 2p_5)(n_n + n_p)] . \end{aligned} \quad (26)$$

Note that  $Q_{nn} \neq Q_{pp}$  except in the case that  $n_n = n_p$ .

A Hartree-Fock calculation of finite nuclei using the bulk Hamiltonian density in Eq. (21) augmented by gradient, Coulomb and spin-orbit terms is more complicated than that using the Skyrme-like Hamiltonian in Eq. (2) because of terms that vary exponentially with density in Eq. (21). Therefore, we have fit the APR equation of state for bulk nuclear and neutron matter up to 3/2 nuclear matter density to that of a Skyrme-like Hamiltonian. For a realistic description of nuclei, the density dependence of the effective masses is important, so we have constrained the fit so that the effective masses match as closely as possible those of the APR equation of state. We have also adjusted the coefficient of the spin-orbit interaction so as to closely match the charge radii and binding energies of <sup>208</sup>Pb, <sup>90</sup>Zr, and <sup>40</sup>Ca. This procedure leads to the parameter set given in Table II and is referred to as NRAPR below. Figure 2 shows that in matter a good fit to the exact APR binding energy/particle is obtained. A fit was also made using the field-theoretical approach, referred to as RAPR, and the parameters are tabulated in Table III. As shown in Fig. 2 the fit is even a little better than in the non-relativistic case.

TABLE II: Parameters for the Skyrme Hamiltonian obtained from a fit to the EOS given by the APR Hamiltonian, Eq. (21); the dimensions are such that  $\mathcal{H}$  is in MeV fm<sup>-3</sup>. This model is referred to as NRAPR in the text.

$t_0$	$t_1$	$t_2$	$t_3$	$x_0$
-2719.7	417.64	-66.687	15042	0.16154
$x_1$	$x_2$	$x_3$	$\epsilon$	$W_0$
-0.047986	0.027170	0.13611	0.14416	41.958

It is difficult to utilize these low-density fits to APR at densities of relevance to neutron stars, largely because of the phase transition that is present in APR. There is not enough freedom in either the present potential model approach or the field-theoretical approach to simultaneously match the equation of state at low densities and satisfy the constraint on the maximum mass neutron star. We have also attempted fitting the low-density and high-density phases of APR separately. Although this is somewhat difficult to accomplish with the field-theoretical model above, it is easily done

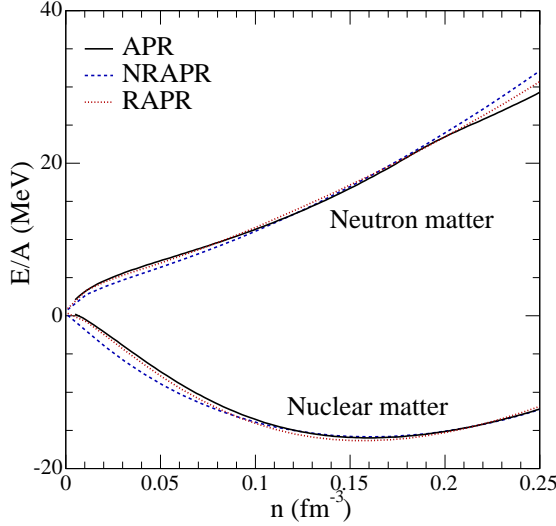


FIG. 2: Binding energy per particle versus density in nuclear matter and neutron matter for the EOS's of APR (solid line), NRAPR (dashed line), and RAPR (dotted line).

TABLE III: Coupling strengths for the Lagrangian in Eq. (13) that fit the APR Hamiltonian density in Eq. (21) up to 3/2 nuclear matter density; the dimensions of  $a_i$  and  $b_i$  are such that  $\mathcal{L}$  is in MeV<sup>4</sup>. This model is referred to as RAPR in the text.

$m_\sigma$	$g_\sigma$	$g_\omega$	$g_\rho$	$\kappa$	$\lambda$
494.28 MeV	7.8144	9.2629	10.288	4.3789 MeV	0.078205
$\zeta$	$\xi$	$a_1$	$a_2$	$a_3$	$a_4$
0.065381	0.30524	0.18566	0.73588	$7.5995 \times 10^{-3}$	$3.4620 \times 10^{-4}$
$a_5$	$a_6$	$b_1$	$b_2$	$b_3$	
$6.7880 \times 10^{-6}$	$5.4824 \times 10^{-8}$	0.039169	$3.1323 \times 10^{-9}$	$9.8907 \times 10^{-10}$	

with the potential model. However, this patchwork approach falls outside our goal of studying correlations that are generic to equations of state without softening phase transitions. In what follows, therefore, results for nuclei are calculated using the NRAPR and RAPR models, whereas those for neutron stars are from calculations using the original EOS of APR.

### III. SEMI-INFINITE NUCLEONIC MATTER

The isospin dependence of the nuclear force has its most important ramifications in the bulk and surface energies of nuclei. In finite nuclei, these effects are coupled, but certain properties like the neutron skin thickness are affected more by the surface effects. The role of the surface is most easily ascertained by an investigation of semi-infinite matter [26, 27]. In this case, matter is assumed to vary only along one axis (the  $z$ -axis) and is assumed to be uniform in the two remaining spatial directions. Matter at the  $z \rightarrow -\infty$  limit is saturated matter at a specified proton fraction, whereas the  $z \rightarrow +\infty$  limit is the vacuum (see Fig. 3). Matter in these two limits are in chemical and pressure equilibrium with each other. Thus, matter in the  $z \rightarrow -\infty$  limit is at the saturation density for the reference proton fraction, with vanishing pressure.

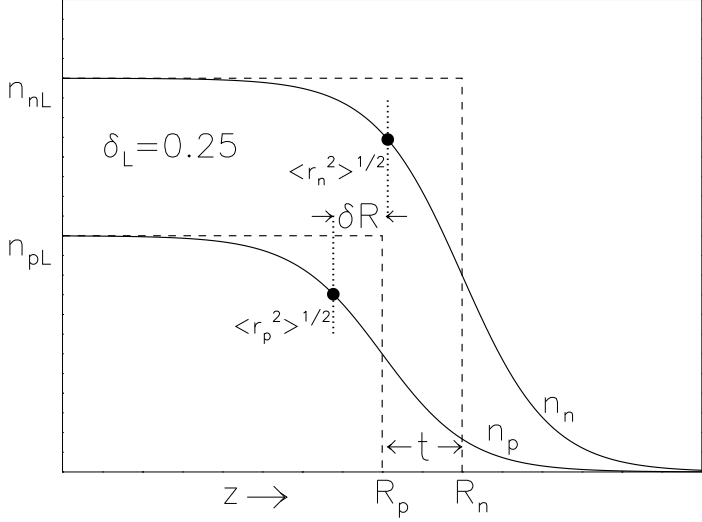


FIG. 3: Schematic diagram of the surface regions of semi-infinite matter indicating the relation between the neutron skin thickness,  $\delta R$ , and the corresponding quantity  $t = R_n - R_p$  determined from the squared-off neutron and proton density distributions.

We note that in sufficiently neutron-rich matter, such as neutron star matter, the (non-relativistic) chemical potential for neutrons at the saturation density is positive. In this situation, which occurs when the reference proton fraction is less than about 0.35, the pressure at the saturation density will also be positive and there must be a finite density of neutrons in the  $z \rightarrow +\infty$  region with the same pressure and neutron chemical potential.

We will study how the surface energy and the neutron skin thickness vary in the semi-infinite approximation due to modifications of nuclear model parameters (including those that delineate isospin effects). These features can be connected to experimental properties of laboratory nuclei.

### A. Variational Approach

The density profiles of semi-infinite matter (schematically illustrated in Fig. 3) are obtained by minimizing the Hamiltonian (energy) density subject to the constraints of baryon number and charge conservation. The baryon and isospin asymmetry densities,

$$n = n_n + n_p, \quad \alpha = n_n - n_p, \quad (27)$$

respectively (and fields and functions of them), are  $z$ -dependent even though we do not explicitly indicate them as such. The neutron excess is defined by  $\delta = \alpha/n$ . We will denote quantities at  $z = -\infty$  by the use of the subscript “ $L$ ”. Primes will generally indicate derivatives with respect to the coordinate  $z$ . Pressure equilibrium between the dense nuclear phase and the vacuum requires that the pressure  $P_L = 0$ . Therefore, the density  $n_L$  is the saturation density for matter with a neutron excess  $\delta_L$ . The value of  $n_L$ , the surface profiles  $n_n$  and  $n_p$ , and the surface energy (to be defined below), are all determined for a given nuclear force model by the single quantity  $\delta_L$ .

We denote the saturation density of symmetric matter by  $n_0 \equiv n_L(\delta_L = 0)$ . The symmetry energy function  $E_{sym}(n)$  is generally a function of density and temperature  $T$ , but we consider only  $T = 0$  matter in this paper. For isospin symmetric matter  $E_{sym}(n_0) \equiv S_v$  is the standard volume symmetry energy parameter whose value lies in the range 25–35 MeV. We also define the squared-off neutron and proton radii (see Fig. 3),  $R_n$  and  $R_p$ , by

$$n_{nL}(R_n - L) = \int_{-L}^{\infty} n_n \, dz \quad ; \quad n_{pL}(R_p - L) = \int_{-L}^{\infty} n_p \, dz, \quad (28)$$

where  $L \rightarrow \infty$ . Although these integrals formally diverge, the quantities  $R_n$  and  $R_p$  are finite.

The variation of the Hamiltonian density

$$\delta \int_{-\infty}^{\infty} [\mathcal{H} - \mu n - \mu_\alpha \alpha] \, dz = 0 \quad (29)$$

results in the two Euler-Lagrange equations

$$\frac{\partial \mathcal{H}}{\partial n} - \mu = \frac{d}{dz} \frac{\partial \mathcal{H}}{\partial n'}, \quad (30)$$

$$\frac{\partial \mathcal{H}}{\partial \alpha} - \mu_\alpha = \frac{d}{dz} \frac{\partial \mathcal{H}}{\partial \alpha'}, \quad (31)$$

where  $2\mu = \mu_n + \mu_p$  and  $2\mu_\alpha = \mu_n - \mu_p$  are the Lagrange multipliers (equivalently, chemical potentials) associated with the constraints of baryon number and charge conservation, respectively. These chemical potentials are related to the individual neutron and proton chemical potentials through  $\mu n + \mu_\alpha \alpha = \mu_n n_n + \mu_p n_p$ .

For Hamiltonians of the form of Eq. (1), without  $\mathcal{H}_C$  and  $\mathcal{H}_J$ , we find

$$\begin{aligned} \frac{\partial \mathcal{H}_B}{\partial n} - \mu &= \frac{n''}{4} (Q_{nn} + 2Q_{np} + Q_{pp}) + \frac{\alpha''}{4} (Q_{nn} - Q_{pp}) \\ &\quad + \frac{1}{8} \left[ 2 \frac{\partial Q_{np}}{\partial n} \left( (n')^2 + (\alpha')^2 \right) + \left( \frac{\partial Q_{nn}}{\partial n} + \frac{\partial Q_{pp}}{\partial n} \right) \left( (n')^2 - (\alpha')^2 \right) \right. \\ &\quad \left. + 2 \left( \frac{\partial Q_{nn}}{\partial \alpha} + 2 \frac{\partial Q_{np}}{\partial \alpha} + \frac{\partial Q_{pp}}{\partial \alpha} \right) n' \alpha' + 2 \left( \frac{\partial Q_{nn}}{\partial \alpha} - \frac{\partial Q_{pp}}{\partial \alpha} \right) (\alpha')^2 \right], \end{aligned} \quad (32)$$

$$\begin{aligned} \frac{\partial \mathcal{H}_B}{\partial \alpha} - \mu_\alpha &= \frac{\alpha''}{4} (Q_{nn} - 2Q_{np} + Q_{pp}) + \frac{n''}{4} (Q_{nn} - Q_{pp}) \\ &\quad - \frac{1}{8} \left[ 2 \frac{\partial Q_{np}}{\partial \alpha} \left( (n')^2 + (\alpha')^2 \right) + \left( \frac{\partial Q_{nn}}{\partial \alpha} + \frac{\partial Q_{pp}}{\partial \alpha} \right) \left( (n')^2 - (\alpha')^2 \right) \right. \\ &\quad \left. - 2 \left( \frac{\partial Q_{nn}}{\partial n} - 2 \frac{\partial Q_{np}}{\partial n} + \frac{\partial Q_{pp}}{\partial n} \right) n' \alpha' - 2 \left( \frac{\partial Q_{nn}}{\partial n} - \frac{\partial Q_{pp}}{\partial n} \right) (n')^2 \right]. \end{aligned} \quad (33)$$

Both sides of these equations vanish for  $z \rightarrow \pm\infty$ .

The surface energy is the difference between the total energy and the bulk energy of an equivalent number of neutrons and protons at the saturation density. Equivalently, the surface thermodynamical potential per unit area is expressed [28] by the same integral that is minimized in Eq. (29):

$$\sigma = \int_{-\infty}^{\infty} [\mathcal{H} - \mu n - \mu_\alpha \alpha] \, dz. \quad (34)$$

The quantity  $\sigma$  is also known as the surface tension. The integrand vanishes at  $z \rightarrow \pm\infty$ , expressing the fact that the pressure vanishes there. Expanding  $\sigma(\delta_L)$  in terms of the neutron excess  $\delta_L$

$$\sigma(\delta_L) = \sigma(\delta_L = 0) + \frac{\partial\sigma}{\partial\delta_L^2} \bigg|_{\delta_L=0} \delta_L^2 + \dots \equiv \sigma_0 - \sigma_\delta \delta_L^2 + \dots \quad (35)$$

allows us to identify  $\sigma_\delta$  as the symmetry parameter of the surface tension. We note that the surface *energy* (which is the product of surface tension and a characteristic surface area), as distinct from the surface thermodynamic potential, has a surface symmetry parameter identical to this, but of opposite sign [28].

The neutron skin thickness is defined by

$$t = R_n - R_p = \int_{-\infty}^{\infty} \left( \frac{n_n}{n_{nL}} - \frac{n_p}{n_{pL}} \right) dz. \quad (36)$$

Using the relations

$$n_{nL} = \frac{1}{2}n_L(1 + \delta_L) \quad ; \quad n_{pL} = \frac{1}{2}n_L(1 - \delta_L) \quad (37)$$

the neutron skin thickness can be expressed in the equivalent form

$$t = \frac{2\delta_L}{n_L(1 - \delta_L^2)} \int_{-\infty}^{\infty} n \left( \frac{\delta}{\delta_L} - 1 \right) dz. \quad (38)$$

Were the neutron and proton density distributions describable by Fermi functions defined by half-density radii  $z_{n,p}$  and diffuseness parameters  $a_{n,p}$ :

$$n_{n,p} = \frac{n_{(n,p)L}}{1 + e^{(z-z_{n,p})/a_{n,p}}}, \quad (39)$$

the skin thickness would be  $t \cong z_n - z_p$ , to lowest order in the diffuseness parameters  $a_{n,p}$ . We note that the definition of skin thickness might be problematic in finite nuclei where there are often oscillations of the density profiles near the center. In this case, the skin thickness is better expressed as the difference between the neutron and proton rms radii  $\langle r_{n,p}^2 \rangle^{1/2}$ . To lowest order in diffuseness corrections, one finds that  $\delta R = \langle r_n^2 \rangle^{1/2} - \langle r_p^2 \rangle^{1/2} \cong \sqrt{\frac{3}{5}} t$ .

### 1. Potential Models

The Euler-Lagrange equations (32) and (33), multiplied respectively by  $n'$  and  $\alpha'$ , then added and integrated, yield

$$(Q_{nn} + 2Q_{np} + Q_{pp}) \frac{(n')^2}{8} + (Q_{nn} - 2Q_{np} + Q_{pp}) \frac{(\alpha')^2}{8} + (Q_{nn} - Q_{pp}) \frac{n'\alpha'}{4} = \mathcal{H}_B - \mu n - \mu_\alpha \alpha. \quad (40)$$

This equation holds even in the case in which the  $Q$ 's are density-dependent. The right-hand side of this equation is the bulk thermodynamic potential density,  $\Omega_B/V = -P_B$ , where  $P_B = n^2[\partial(\mathcal{H}_B/n)/\partial n]$  is the bulk pressure. Note from Eq. (40) that the bulk and gradient terms contribute equally to the surface tension in Eq. (34), which can therefore be written as

$$\sigma(\delta_L) = 2 \int_{-\infty}^{\infty} [\mathcal{H}_B - \mu n - \mu_\alpha \alpha] dz. \quad (41)$$

To lowest order the bulk Hamiltonian should be quadratic in the neutron excess  $\delta$ :

$$\mathcal{H}_B = \mathcal{H}_B(n, \delta = 0) + E_{sym}(n)n\delta^2. \quad (42)$$

Since the bulk pressure vanishes for  $z \rightarrow -\infty$ , the chemical potentials, to second order in  $\delta_L$ , are

$$\mu_n = -B + S_v\delta_L(2 - \delta_L), \quad (43)$$

$$\mu_p = -B - S_v\delta_L(2 + \delta_L), \quad (44)$$

where  $B \equiv -\mathcal{H}_B(n_0, \delta = 0)/n_0$  is the symmetric matter bulk binding energy per particle. Therefore the surface tension becomes

$$\sigma(\delta_L) = 2 \int_{-\infty}^{\infty} \left[ \mathcal{H}_B(n, \delta = 0) + n \left( B + \delta^2 E_{sym}(n) + \delta_L^2 S_v - 2\delta\delta_L S_v \right) \right] dz. \quad (45)$$

We are interested in evaluating this in the case that  $\delta_L$  is small so that we can take  $Q_{nn} = Q_{pp}$ ; this is exactly true for standard Skyrme Hamiltonians and approximately so for the APR Hamiltonian. It is also reasonable in this case to use Eq. (40) with  $(\alpha')^2$  set to zero which results in a quadrature formula for the surface density profile:

$$\sqrt{Q_{nn} + Q_{np}} dn = 2\sqrt{\mathcal{H}_B - \mu n - \mu_\alpha \alpha} dz. \quad (46)$$

Utilizing this result, Eq. (45) can now be written as

$$\sigma(\delta_L) = \sqrt{Q_{nn} + Q_{np}} \int_0^{n_L} \left[ \mathcal{H}_B(n, \delta = 0) + n \left( B + \delta^2 E_{sym}(n) + \delta_L^2 S_v - 2\delta\delta_L S_v \right) \right]^{1/2} dn. \quad (47)$$

Again setting  $Q_{nn} = Q_{pp}$ , neglecting derivatives of  $\alpha$  and further assuming that the dependence of the  $Q$ 's on  $\alpha$  can be neglected, the right hand side of Eq. (33) is zero so that

$$4E_{sym}(n)\delta \simeq \mu_n - \mu_p. \quad (48)$$

Using Eqs. (43) and (44) this gives the useful result

$$\frac{\delta}{\delta_L} = \frac{S_v}{E_{sym}(n)}. \quad (49)$$

(Note that the use of Eq. (48), which is strictly valid to order  $\delta$  in bulk matter, requires that the variation of  $\delta$  in the surface tracks its behavior in the bulk.) Substitution of these relations in Eq. (47) yields the quadrature

$$\sigma(\delta_L) = \sqrt{Q_{nn} + Q_{np}} \int_0^{n_L} \left[ \mathcal{H}_B(n, \delta = 0) + nB - nS_v\delta_L^2 \left( \frac{S_v}{E_{sym}(n)} - 1 \right) \right]^{1/2} dn. \quad (50)$$

Then the surface tension of symmetric semi-infinite matter is

$$\sigma_0 \equiv \sigma(\delta_L = 0) = \sqrt{Q_{nn} + Q_{np}} \int_0^{n_L} [\mathcal{H}_B(n, \delta = 0) + nB]^{1/2} dn, \quad (51)$$

and expansion of the argument of the integral in Eq. (50) allows us to write the surface symmetry parameter in the convenient form

$$\sigma_\delta = \frac{S_v}{2} \sqrt{Q_{nn} + Q_{np}} \int_0^{n_L} n \left[ \frac{S_v}{E_{sym}(n)} - 1 \right] [\mathcal{H}_B(n, \delta = 0) + nB]^{-1/2} dn. \quad (52)$$

Our results will be given in terms of the surface energy  $E_s = 4\pi r_0^2 \sigma_0$  and the surface symmetry energy  $S_s = 4\pi r_0^2 \sigma_\delta$ , where  $(4\pi r_0^3/3)(0.16 \text{ fm}^{-3}) = 1$ . It is often useful to eliminate the  $Q$ 's by forming the ratio of Eqs. (52) and (51). This yields

$$\frac{S_s}{S_v} = \frac{E_s}{2} \frac{\int_0^{n_L} n [S_v/E_{sym}(n) - 1] [\mathcal{H}_B(n, \delta = 0) + nB]^{-1/2} dn}{\int_0^{n_L} [\mathcal{H}_B(n, \delta = 0) + nB]^{1/2} dn}. \quad (53)$$

This equation and Eqs. (51) and (52) are central to the results to be presented in Sec. IV below. Finally, the profile equation (40) and the relation for  $\delta$ , Eq. (49), can be employed in the expression (38) to yield the relation

$$t = \frac{1}{n_L} \frac{2\delta_L}{(1 - \delta_L^2)} \frac{\sigma_\delta}{S_v} \quad (54)$$

between the skin thickness and the surface tension that was conceived in the droplet model [29, 30, 31] and later shown [5] to be quite general.

The analytical description of the nuclear surface based on the leptodermous expansion was pioneered by Myers and Swiatecki [29] and developed further in several works [5, 28, 30, 31, 32]. Our analysis here offers a convenient expression for  $S_s/S_v$  (Eq. (53)) in terms of the energy density functional for isospin symmetric infinite nucleonic matter.

## 2. Field Theoretical Models

For spatially non-uniform semi-infinite isospin asymmetric matter, the Euler-Lagrange equations corresponding to the Lagrangian (13) yield the meson and baryon field equations

$$\sigma_0'' = m_\sigma^2 \sigma_0 - g_\sigma n_s + \frac{\kappa}{2} g_\sigma^3 \sigma_0^2 + \frac{\lambda}{6} g_\sigma^4 \sigma_0^3 - g_\rho^2 \rho_0^2 \frac{\partial f}{\partial \sigma_0}, \quad (55)$$

$$\omega_0'' = m_\omega^2 \omega_0 - g_\omega n + \frac{\zeta}{6} g_\omega^4 \omega_0^3 + g_\rho^2 \rho_0^2 \frac{\partial f}{\partial \omega_0}, \quad (56)$$

$$\rho_0'' = m_\rho^2 \rho_0 - \frac{1}{2} g_\rho \alpha + 2g_\rho^2 \rho_0 f + \frac{\xi}{6} g_\rho^4 \rho_0^3, \quad (57)$$

$$0 = (i\partial - g_\omega \omega_0 \gamma_0 + \frac{1}{2} g_\rho \rho_0 \gamma_0 - M + g_\sigma \sigma_0) \psi_n, \quad (58)$$

$$0 = (i\partial - g_\omega \omega_0 \gamma_0 - \frac{1}{2} g_\rho \rho_0 \gamma_0 - M + g_\sigma \sigma_0) \psi_p, \quad (59)$$

where primes indicate derivatives with respect to  $z$ , the subscript “0” indicates that the mean field approximation has been used and  $\rho_0$  refers to the mean field of the neutral rho meson. We shall adopt the Thomas-Fermi approximation since it provides a reasonably accurate simplification of the Hartree approach [26]. Here the meson fields are assumed to vary sufficiently slowly that the nucleons can be regarded as moving in locally constant fields at every point in space. Thus the

Fermi momenta and the effective mass depend upon  $z$ , i.e.,  $k_{F_n}(z)$ ,  $k_{F_p}(z)$  and  $M^*(z)$ . The local neutron, proton and scalar densities at a given  $z$  are then

$$\begin{aligned} n_n &= \frac{k_{F_n}^3}{3\pi^2} ; \quad n_p = \frac{k_{F_p}^3}{3\pi^2} , \\ n_s &= 2 \int_0^{k_{F_n}} \frac{d^3k}{(2\pi)^3} \frac{M^*}{\sqrt{k^2 + M^{*2}}} + 2 \int_0^{k_{F_p}} \frac{d^3k}{(2\pi)^3} \frac{M^*}{\sqrt{k^2 + M^{*2}}} , \end{aligned} \quad (60)$$

respectively. The energy eigenvalues of the Dirac equations for the neutron and proton fields are

$$e_n(k) = \sqrt{k^2 + M^{*2}} + g_\omega \omega_0 - \frac{1}{2} g_\rho \rho_0 ; \quad e_p(k) = \sqrt{k^2 + M^{*2}} + g_\omega \omega_0 + \frac{1}{2} g_\rho \rho_0 , \quad (61)$$

respectively. The local Thomas-Fermi Hamiltonian density is then

$$\begin{aligned} \mathcal{H}(z) &= \frac{1}{2} \left( \sigma_0'^2 + m_\sigma^2 \sigma_0^2 \right) - \frac{1}{2} \left( \omega_0'^2 + m_\omega^2 \omega_0^2 \right) - \frac{1}{2} \left( \rho_0'^2 + m_\rho^2 \rho_0^2 \right) + \frac{\kappa}{6} (g_\sigma \sigma_0)^3 + \frac{\lambda}{24} (g_\sigma \sigma_0)^4 \\ &\quad - \frac{\zeta}{24} (g_\omega \omega_0)^4 - \frac{\xi}{24} (g_\rho \rho_0)^4 - g_\rho^2 \rho_0^2 f + 2 \int_0^{k_{F_n}} \frac{d^3k}{(2\pi)^3} e_n + 2 \int_0^{k_{F_p}} \frac{d^3k}{(2\pi)^3} e_p . \end{aligned} \quad (62)$$

Note that, in contrast to the nonrelativistic case, the energy density is not simply expressible in terms of just the baryon densities and their gradients. The ground state of the system is obtained by minimizing  $\mathcal{H}(z) - \mu_n n_n - \mu_p n_p$  with respect to the local Fermi wavenumbers  $k_{F_n}(z)$  and  $k_{F_p}(z)$ . The Lagrange multipliers (chemical potentials) that fix the number of neutrons and protons are then

$$\mu_n = e_n(k_{F_n}) ; \quad \mu_p = e_p(k_{F_p}) . \quad (63)$$

The algebraic nature of these two coupled equations relating the neutron and proton density profiles to the meson fields stems from the Thomas-Fermi approximation.

In order to obtain the density profiles  $n_n(z)$  and  $n_p(z)$ , Eqs. (55)–(57) and (63) are supplemented by the boundary conditions

$$\left. \begin{aligned} \sigma_0(-L) &= \sigma_{0L} , & \omega_0(-L) &= \omega_{0L} , & \rho_0(-L) &= \rho_{0L} , \\ \sigma_0(L) &= 0 , & \omega_0(L) &= 0 , & \rho_0(L) &= 0 , \end{aligned} \right\} L \rightarrow \infty$$

where the subscript “ $0L$ ” indicates values of the fields in equilibrium at the specified neutron excess  $\delta_L$ . (Note that the meson fields are finite, but exponentially small, in regions of space where the baryon density vanishes as prescribed by the Thomas-Fermi approximation.) These conditions guarantee that the derivatives of the fields vanish at the boundaries. In practice, we impose these conditions at points  $(-L, L)$  that are sufficiently far from the surface to ensure that the surface energy is unchanged by small variations in  $L$ .

The numerical solution of the differential equations requires some care because of their behavior at the boundaries. We find it best to use a relaxation method. Starting with small values for the field derivatives, we integrate from  $-L$  outwards. The integration has to be stopped when one of the fields becomes negative, say at  $L_1 > -L$ . This solution can then be used as an initial guess for relaxation in the region  $(-L_2, L_2)$ , where  $L_2 = (L_1 + L)/2$ . After convergence is obtained,  $L_2$  can be increased by a small amount and the relaxation applied again until the field derivatives are sufficiently small to ensure that the surface tension remains stationary.

The determination of the density profiles enables the calculation of the surface tension. In the non-relativistic case Eq. (40) showed that the bulk and gradient terms in the Hamiltonian

density gave equal contributions to the surface tension. A similar result can be obtained here by multiplying Eqs. (55)–(57) by the derivative of the appropriate field with respect to  $z$ , combining the equations and integrating. This gives

$$\mathcal{H}_B - \mu n - \mu_\alpha \alpha = \frac{1}{2} \left( \sigma'_0{}^2 - \omega'_0{}^2 - \rho'_0{}^2 \right) , \quad (64)$$

where  $\mathcal{H}_B$  denotes the bulk Hamiltonian, namely the non-derivative terms in Eq. (62). Thus we can employ Eq. (41) to calculate the surface tension here also. However, it is not possible to reduce the calculation of the surface energy to a simple quadrature over the density since here derivatives of three fields are involved. Note that in the relativistic case the  $Q$ 's are the coefficients of the field gradients with

$$Q_{\sigma\sigma} = -Q_{\omega\omega} = -Q_{\rho\rho} = 1 , \quad (65)$$

all other coefficients being zero.

## B. Relationship to the Liquid Droplet Model of Nuclei

The empirical liquid droplet approach, originally formulated in Ref. [29], provides a useful framework for the description of nuclei in the equation of state relevant for astrophysical simulations of supernovae and neutron stars. The droplet approach for isolated nuclei can be easily extended to the case in which nuclei are immersed in a dense medium comprised of electrons, positrons, protons, neutrons and alpha particles [28]. Historically, the parameters of the droplet model have been established from fits to binding energy data for laboratory nuclei (cf., Ref. [29]). Although such fits cannot independently establish reliable values for the volume and surface symmetry coefficients, they can determine a strong correlation between them. This correlation, however, depends on the formulation of the droplet model.

The simplest droplet model consists of an extension of the Bethe-von Weizsäcker liquid drop model to incorporate the surface asymmetry. As demonstrated by Myers and Swiatecki [29], the nuclear energy can be written as

$$\begin{aligned} E(A, Z) = & -BA + E_s A^{2/3} + S_v A \frac{(1 - 2Z/A)^2}{1 + (S_s^* A^{-1/3} / S_v)} + E_C \frac{Z^2}{A^{1/3}} \\ & + E_{dif} \frac{Z^2}{A} + E_{ex} \frac{Z^{4/3}}{A^{1/3}} + a \Delta A^{-1/2} . \end{aligned} \quad (66)$$

In this expression,  $B \simeq 16$  MeV is the binding energy per particle of bulk symmetric matter at saturation,  $E_s, E_C, E_{dif}$  and  $E_{ex}$  are coefficients for the surface energy of symmetric matter, the Coulomb energy of a uniformly charged sphere, the diffuseness correction and the exchange correction to the Coulomb energy, respectively. The last term represents pairing corrections, where  $\Delta$  is a constant and  $a = +1$  for odd-odd nuclei, 0 for odd-even nuclei, and  $-1$  for even-even nuclei. The effects of curvature and higher-order terms are neglected. The quantity  $S_s^*$  is related to  $S_s$  as described below.

Care must be taken in making the assumption that the surface energy scales as  $A^{2/3}$  and the Coulomb energy as  $Z^2 A^{-1/3}$ . Physically, the Coulomb energy scales as  $Z^2 / R_p$ . The surface energy scales with the surface area, but its definition depends on the exact radius of the surface and is therefore ambiguous [28]. Nevertheless, the total of the bulk plus surface energies is unambiguous. This ambiguous splitting of the bulk and surface energies can be resolved if the surface thermodynamic potential is used instead of the surface energy. In what follows, we describe two ways in which this can be done.

### 1. “ $\mu_n$ ” Approach

In this approach developed by Lattimer et al. [28],  $R_p$  is used as the reference surface. This choice was made since the Coulomb energy is naturally expressed in terms of this radius. Since, in general,  $R_n > R_p$ , the bulk energy of an additional  $N_s$  neutrons in the neutron skin has to be included. The diffuseness and Coulomb exchange corrections are also naturally expressed in terms of  $R_p$ . These definitions allow the mass formula to be simply written in terms of the variables  $A$  and  $I = 1 - 2Z/A$ . However, the connection between  $R_p$  and  $A$  depends on the density (assumed to be uniform and equal to  $n_L$ ) of the bulk interior fluid. This results in the modified surface symmetry energy parameter

$$S_s^* = 4\pi \left( \frac{3}{4\pi n_0} \right)^{2/3} \sigma_\delta \quad (67)$$

where the true saturation density  $n_0$  is used in place of the fiducial density of  $0.16 \text{ fm}^{-3}$ . Different parameterizations of the nuclear force predict different values for the saturation density, and consequently for the interior densities  $n_L$  in nuclei. Using  $R$  to refer to  $R_p$  in this approach, the total droplet energy becomes

$$\begin{aligned} E(A, Z) = & (-B + S_v \delta_L^2)(A - N_s) + 4\pi R^2 \sigma(\mu_n^s) + \mu_n^s N_s \\ & + \frac{3Z^2 e^2}{5R} - \frac{\pi^2 Z^2 e^2 d^2}{2R^3} - \frac{3Z^{4/3} e^2}{4R} \left( \frac{3}{2\pi} \right)^{2/3} + a \Delta A^{-1/2}, \end{aligned} \quad (68)$$

where explicit expressions for  $E_C$ ,  $E_{dif}$  and  $E_{ex}$  have been substituted. The quantity  $d \approx 0.55 \text{ fm}$  is the surface diffuseness parameter. Note that the bulk energy per baryon in the interior, expanded to second order in  $\delta_L$ , is  $-B + S_v \delta_L^2$ , and that the total surface energy is  $4\pi R^2 \sigma(\mu_n^s) + \mu_n^s N_s$ , where the surface thermodynamic potential per unit area  $\sigma$  is a function of the surface neutron chemical potential  $\mu_n^s$ . Technically, the surface tension is a function of both  $\mu_n$  and  $\mu_p$ , but if Coulomb and other finite-size effects are neglected, the matter pressure vanishes throughout the surface and  $\mu_n$  and  $\mu_p$  can each be expressed as a unique function of  $\delta_L$ . Thus, the surface tension in this limit can be expressed as a function of only one chemical potential. Since by definition only neutrons exist in the neutron skin, it is appropriate to take the surface tension as a function of  $\mu_n$ . Minimizing the total energy with respect to  $\mu_n^s$  requires that  $\mu_n$  be the same in the surface as in the bulk interior, and its value is thus given by Eq. (43). The function  $\sigma(\mu_n^s)$  is determined through the auxiliary variable  $\delta_L$  using  $\sigma = \sigma_0 - \sigma_\delta \delta_L^2$ . The number of surface neutrons follows from minimizing the total energy with respect to  $N_s$  and leads to the thermodynamic identity

$$N_s = -4\pi R^2 \frac{\partial \sigma(\mu_n)}{\partial \mu_n} = 4\pi R^2 \frac{\sigma_\delta \delta_L}{S_v(1 - \delta_L)}. \quad (69)$$

Noting that the local asymmetry in the bulk interior is

$$\delta_L = \frac{A - N_s - 2Z}{A - N_s}, \quad (70)$$

one has that  $N_s = A(I - \delta_L)/(1 - \delta_L)$ , where the global asymmetry is  $I = (N - Z)/A$ . Thus, it is possible to establish that

$$\delta_L = I \left[ 1 + \frac{4\pi R^2 \sigma_\delta}{S_v A} \right]^{-1}. \quad (71)$$

In order to express the modified liquid droplet energy in terms of  $A$  and  $I$ , it is necessary to relate the nuclear proton radius  $R$  to  $A$ , the interior density  $n_L$  and the asymmetry  $I$ . This is accomplished with the implicit relation

$$\frac{4\pi}{3}R^3n_L = A - N_s = A\frac{1 - I}{1 - \delta_L} = A(1 - I)\left[1 - \frac{AI}{A + 4\pi R^2\sigma_\delta/S_v}\right]^{-1}. \quad (72)$$

This is a quintic equation for  $R$ . It is convenient to write its solution in terms of a function  $v(A, I, n_L)$  such that

$$R = r_0[A v(A, I, n_L)(0.16 \text{ fm}^{-3})n_L^{-1}]^{1/3}, \quad (73)$$

where, as before,  $(4\pi r_0^3/3)(0.16 \text{ fm}^{-3}) = 1$ . We also define  $S_s = 4\pi r_0^2\sigma_\delta$  to provide a measure of the surface symmetry parameter that is independent of the interior density, unlike  $S_s^*$  in the simple liquid droplet model. In the case of symmetric matter, the quantity  $v(A, I, n_L)$  would simply equal unity; for asymmetric matter, it also contains the effects of the neutron skin. The implicit equation for  $v$  becomes

$$(v - 1)(1 + \alpha v^{2/3} - I) = -\alpha I v^{2/3}, \quad (74)$$

where

$$\alpha = \frac{S_s}{S_v A^{1/3}} \left( \frac{0.16 \text{ fm}^{-3}}{n_L} \right)^{2/3}. \quad (75)$$

In practice, solving the quintic equation for  $v$  can be avoided by employing its expansion

$$v = 1 - \frac{\alpha}{1 + \alpha}I - \frac{\alpha}{(1 + \alpha)^3} \left(1 + \frac{1}{3}\alpha\right) I^2 - \frac{\alpha}{(1 + \alpha)^5} \left(1 + \frac{2}{3}\alpha + \frac{2}{3}\alpha^2 + \frac{1}{9}\alpha^3\right) I^3 + \dots \quad (76)$$

in terms of the small quantity  $I$ . Eliminating  $N_s, \delta_L$  and  $R$ , and setting  $w = v(0.16 \text{ fm}^{-3})/n_L$ , the liquid droplet mass formula becomes

$$\begin{aligned} E(A, Z) = & -BA + 4\pi r_0^2\sigma_0(wA)^{2/3} + S_v A I^2 \left[1 + \frac{S_s w^{2/3}}{S_v A^{1/3}}\right]^{-1} + \frac{3e^2 Z^2}{5r_0} \left(\frac{1}{wA}\right)^{1/3} \\ & - \frac{\pi^2 Z^2 e^2 d^2}{2r_0^3 w A} - \frac{3Z^{4/3} e^2}{4r_0} \left(\frac{3}{2\pi}\right)^{2/3} \left(\frac{1}{wA}\right)^{1/3} + a\Delta A^{-1/2}. \end{aligned} \quad (77)$$

For a given  $A$  and  $Z$ , therefore, the modified liquid droplet energy is a function of the six parameters  $B, \sigma_0, S_v, S_s, n_L$  and  $\Delta$ . The neutron skin thickness is given by

$$t = \frac{2}{3} \frac{r_0 w}{v} \frac{S_s}{S_v} \frac{\delta_L}{1 - \delta_L^2} \quad \text{with} \quad \delta_L = I \left[1 + \frac{S_s w^{2/3}}{S_v A^{1/3}}\right]^{-1}. \quad (78)$$

A shortcoming of the droplet model described above is it employs the surface tension along the coexistence curve for which the pressure is zero and Coulomb effects are ignored. Thus, in a nucleus with  $N = Z$ , it predicts that there should be no neutron skin. However, the Coulomb repulsion of protons results in a lowering of the proton density inside the nucleus and the development of a proton skin. The following section describes the approach adopted by Danielewicz [33] to incorporate this Coulomb effect in the droplet model.

## 2. “ $\mu_\alpha$ ” Approach

In this approach, the surface tension is parameterized in terms of  $\mu_\alpha \equiv (\mu_n - \mu_p)/2$  instead of  $\mu_n$ . The quantity  $\mu_\alpha$  is antisymmetric in neutrons and protons. In this way, the physical feature that the proton chemical potentials in the two bulk phases across a boundary differ is captured. Since neutrons and protons are treated symmetrically, the surface term  $\mu_n^s N_s$  in the mass formula (68) is replaced by

$$(\mu_n^s + \mu_p^s)(N_s + Z_s)/2 + (\mu_n^s - \mu_p^s)(N_s - Z_s)/2. \quad (79)$$

The surface thermodynamic potential is to be treated as function of  $\mu_\alpha^s$  alone. A result of these definitions is that minimization of the total energy with respect to  $\mu_n^s - \mu_p^s$  and  $\mu_n^s + \mu_p^s$  results in the surface asymmetry density being proportional to  $N_s - Z_s \propto \partial\sigma/\partial\mu_\alpha^s$ , whereas the total surface density is proportional to  $N_s + Z_s \propto \partial\sigma/\partial\mu^s$  and will vanish. Thus,  $Z_s = -N_s$  in this approach. In addition, the nuclear radius now satisfies  $4\pi R^3 n_L/3 = A$ .

The possibility that  $Z_s$  protons exist in the surface must be taken into account in the Coulomb energy. Then the Coulomb energy becomes

$$\frac{3e^2}{5R} \left[ Z^2 - \frac{ZZ_s}{3} + \dots \right], \quad (80)$$

to which diffuseness and Coulomb exchange corrections must be added. We note that Danielewicz [33] kept an additional term in the expansion in  $Z_s/Z$ , but this has only a marginal effect on the results. Minimizing the total energy

$$\begin{aligned} E(A, Z) = & (-B + S_v \delta_L^2)(A - N_s - Z_s) + 4\pi R^2 \sigma(\mu_\alpha^s) + \mu^s(N_s + Z_s) + \mu_\alpha^s(N_s - Z_s) \\ & + \frac{3Z^2 e^2}{5R} \left( 1 - \frac{Z_s}{3Z} \right) - \frac{\pi^2 Z^2 e^2 d^2}{2R^3} - \frac{3Z^{4/3} e^2}{4R} \left( \frac{3}{2\pi} \right)^{2/3} + a\Delta A^{-1/2}, \end{aligned} \quad (81)$$

with respect to  $N_s - Z_s$  results in

$$\mu_\alpha^s = 2S_v \delta_L - \frac{e^2 Z}{10R}. \quad (82)$$

Using

$$\sigma = \sigma_0 - \sigma_\delta (\mu_\alpha^s / 2S_v)^2, \quad (83)$$

one finds that

$$\begin{aligned} N_s - Z_s &= 4\pi R^2 \sigma_\delta \frac{\mu_\alpha^s}{2S_v^2} = \alpha A (\delta_L - \beta) \\ &= A(I - \delta_L) = \alpha A \frac{I - \beta}{1 + \alpha}, \end{aligned} \quad (84)$$

$$\delta_L = \frac{I + \alpha\beta}{1 + \alpha}, \quad (85)$$

where  $\alpha = 4\pi R^2 \sigma_\delta / (S_v A)$  has the same definition as in Eq. (75) and  $\beta = e^2 Z / (20RS_v)$ . The neutron skin thickness is

$$t = R_n - R_p = \frac{2}{3} R \frac{N_s - Z_s}{A(1 - \delta_L^2)} = \frac{2}{3} \frac{r_0}{u_0} \frac{S_s}{S_v} \frac{\delta_L - \beta}{1 - \delta_L^2}, \quad (86)$$

where  $u_0 = n_L/0.16 \text{ fm}^{-3}$ . This shows explicitly how the Coulomb repulsion reduces the skin thickness. Finally, the total energy can be written as

$$E(A, Z) = -BA + 4\pi r_0^2 \sigma_0 \left( \frac{A}{u_0} \right)^{2/3} + S_v A \frac{I^2 + \alpha\beta(2I - \beta)}{1 + \alpha} + \frac{3e^2 Z^2}{5r_0} \left( \frac{u_0}{A} \right)^{1/3} \left[ 1 - \frac{5\pi^2 d^2}{6r_0^2} \left( \frac{u_0}{A} \right)^{2/3} - \frac{5}{4} \left( \frac{3}{2\pi Z} \right)^{2/3} \right] + a\Delta A^{-1/2}. \quad (87)$$

## IV. RESULTS

### A. Selection of Models and Their Parameters

In this section, we wish to establish some generic trends that emerge from calculations based on the potential model Hamiltonian in Eq. (2) and the field theoretical Lagrangian in Eq. (13). Toward this end, the various coupling strengths that enter in these two approaches are chosen so as to reproduce the empirical properties of

$$\begin{aligned} \text{equilibrium binding energy} : B &= -16 \pm 1 \text{ MeV}, \\ \text{equilibrium density} : n_0 &= 0.16 \pm 0.01 \text{ fm}^{-3}, \\ \text{incompressibility} : K &= (200 - 300) \text{ MeV}, \\ \text{Landau effective mass} : m_L^* &= (0.6 - 1.0) M, \quad \text{and} \\ \text{symmetry energy} : S_v &= (25 - 35) \text{ MeV}. \end{aligned} \quad (88)$$

In the case of potential models, calculations of nuclei are performed using the Hartree-Fock-Bogoliubov approach [21] that includes pairing interactions. Hartree calculations [34] are employed in the field theoretical approach, as a treatment of the exchange (Fock) terms is considerably more complicated than in the potential model approach. In both approaches, we require that the binding energy and the charge radii of closed-shell nuclei are reproduced to within 2% of the measured values. The scalar meson mass in the field theoretical approach was restricted to lie between 450 and 550 MeV. Insofar as fits to the valence single particle energies of closed shell nuclei are known to require a detailed treatment of correlations beyond the mean field level (such as short range and RPA correlations [35] that are not considered here) we have chosen to tolerate slight deviations from the measured energies. We note, however, that Todd and Piekarewicz [36] have discussed a correlation between the neutron radius of lead and the binding energy of the valence orbitals. They found that smaller neutron radii lead to last occupied neutron orbitals that are more weakly bound, and therefore smaller neutron drip densities.

In all cases considered the supranuclear EOS was constrained to yield a maximum neutron star mass of at least  $1.44M_\odot$ , the larger of the accurately measured neutron star masses in the double neutron star binary PSR1913+16 (see Ref. [37] for a compilation of known masses). This constraint resulted in the elimination of several non-relativistic models in which either the pressure decreased as a function of increasing density (e.g. SkP [38]) or the proton (and hence the electron) fraction vanished at a finite supranuclear density (e.g. SkT3 [39]). In the latter case, the condition of beta-equilibrium requires positrons and anti-protons which potential models cannot account for in a natural manner. Recently, a systematic study of potential models has been performed by Stone et al. [40] who adopt a similar procedure to select among 87 Skyrme parameterizations. In addition to imposing the constraints in Ref. [40] for potential models, we have also removed all models that do not have reasonable values for the Landau parameters at saturation density [41].

Since few relativistic models meet our criteria, we have generated a new class of relativistic models, es25, es275, es30, es325 and es35 with the Lagrangian of Eq. (13). In these models only  $a_2$  and  $b_1$  in Eq. (15) were allowed to be non-zero. They were designed to meet our restrictions while offering some variation in the value of the symmetry energy. We have also exploited the full freedom of the function  $f$  in Eq. (15) to produce models SR1, SR2 and SR3 for which the symmetry energy has a substantially weaker density dependence than in typical relativistic models. This leads to a smaller skin thickness. Note that es25 and es275 also have smaller skin thicknesses than typical.

A list of all of the models used in this work together with their saturation properties, surface energies, and skin thicknesses is given in Table V in Appendix A. In Appendix B the coupling strengths of models SR2, es25, es30, and es35 are listed in Tables VI, VII, VIII, and IX, respectively.

### Results for the EOS of APR

We present here results for nuclei and semi-infinite matter obtained with the potential (NRAPR) and field-theoretical (RAPR) model fits to the EOS of APR. These models satisfy all of the constraints mentioned above. The values obtained for the binding energy/particle and the charge radii of closed-shell nuclei are given in Table IV. The results of the two models differ by at most a few percent and compare quite well with the data. This agreement is gratifying insofar as the EOS of APR was obtained from many-body theory without reference to nuclei. The experimental situation regarding skin thickness is quite model dependent and we show a few representative values in Table IV. In agreement with the prediction, most of the recent extracted values for the skin thickness in  $^{40}\text{Ca}$  are small and negative (however positive values were obtained in earlier work, see the review of Batty et. al. [42]). For  $^{90}\text{Zr}$  the skin thickness is predicted to be 0.084, on average, which is close to the central experimental value. In  $^{208}\text{Pb}$  the theoretical value  $\sim 0.2$  is at the upper end of current experimental estimates.

TABLE IV: Comparison of results from the potential and field theoretical approximations to the APR equation of state with experimental data for selected closed-shell nuclei.

Nucleus	Property	Experiment	Potential	Field-theoretical
$^{208}\text{Pb}$	Charge radius (fm)	5.50 [43]	5.41	5.41
	Binding energy per particle (MeV)	7.87 [44]	7.87	7.77
	Skin thickness (fm)	$0.12 \pm 0.05, 0.20 \pm 0.04$ [10, 45]	0.19	0.20
$^{90}\text{Zr}$	Charge radius (fm)	4.27 [43]	4.18	4.17
	Binding energy per particle (MeV)	8.71 [44]	8.88	8.65
	Skin thickness (fm)	$0.09 \pm 0.07$ [46]	0.075	0.093
$^{40}\text{Ca}$	Charge radius (fm)	3.48 [43]	3.40	3.34
	Binding energy per particle (MeV)	8.45 [44]	8.89	8.61
	Skin thickness (fm)	$-0.06 \pm 0.05, -0.05 \pm 0.04$ [10, 47]	-0.044	-0.046

In Fig. 4 the neutron and proton density distributions for  $^{208}\text{Pb}$  calculated with the NRAPR and RAPR models are seen to agree reasonably well with each other. These results are compared with the corresponding results of semi-infinite matter calculations which also agree reasonably well amongst themselves. There is, however, a noticeable enhancement of the relativistic densities compared to the non-relativistic ones at the onset of the surface region ( $r \sim 5.3$  fm). In order to

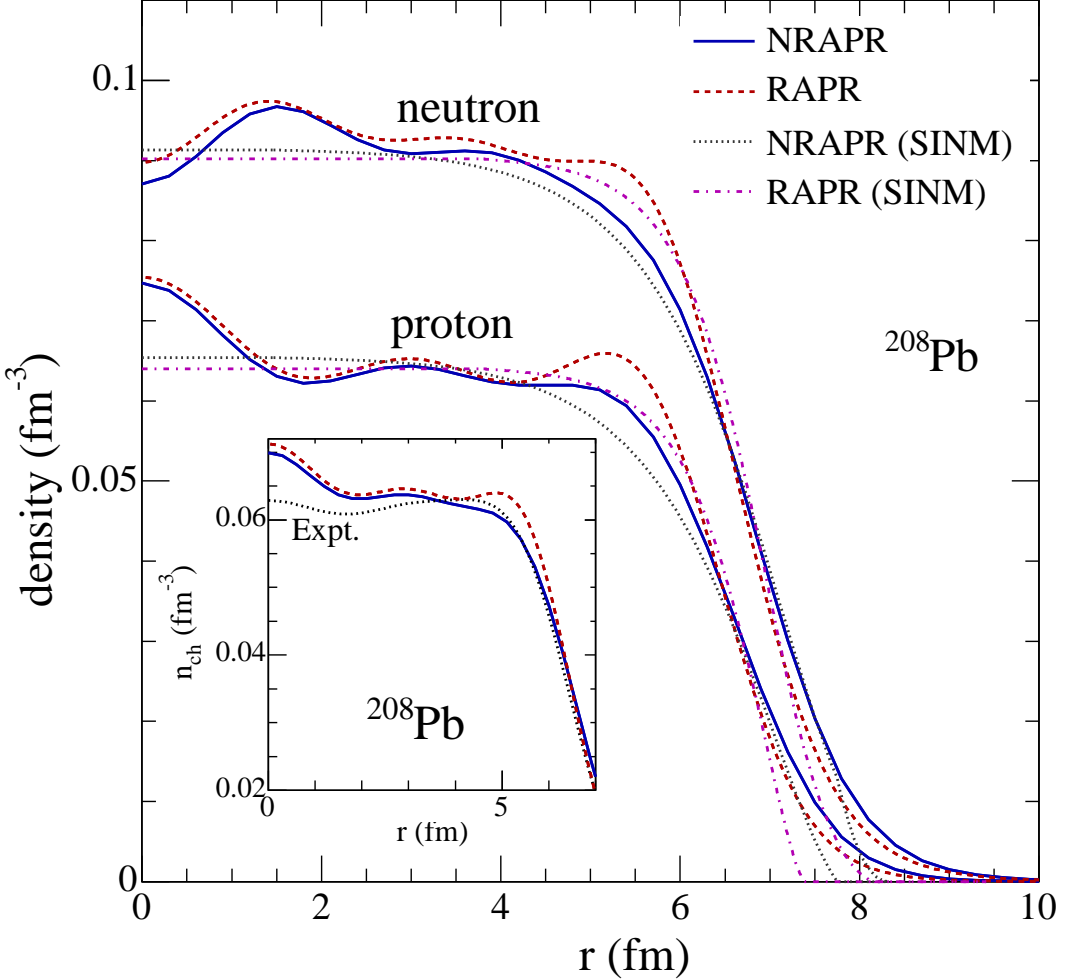


FIG. 4: Calculated neutron and proton density distributions for  $^{208}\text{Pb}$  and for semi-infinite matter. The inset compares the calculated charge distributions with data [48].

specify  $\delta_L$  for the semi-infinite matter calculation, the neutron and proton densities were averaged from the center of the lead nucleus (for each case) out to  $2/3$  of its rms charge radius. This procedure smooths the oscillations in the calculated density distributions and roughly takes into account the effects of short range and RPA correlations [35]. Note that semi-infinite matter calculations in the Thomas Fermi approximation are inherently unreliable in the tail of the distribution. The inset shows that the comparison between the calculated charge distributions and the data [48] is comparable to that of other calculations performed at the Hartree-Fock-Bogoliubov (for potential models) or Hartree (for field-theoretical models) mean field level [15, 22].

Figure 5 shows neutron and proton density profiles from semi-infinite matter calculations for a range of  $\delta_L$ 's for the NRAPR and RAPR fits to the EOS of APR. The isospin dependence of the profiles generally matches well with that of the semi-infinite matter profiles calculated directly from the EOS of APR. Values of  $\delta_L$  larger than about 0.3 (not considered for the RAPR case) necessitate the presence of dripped neutrons since the neutron chemical potential is positive. Hence the neutron density remains finite as  $z \rightarrow \infty$ .

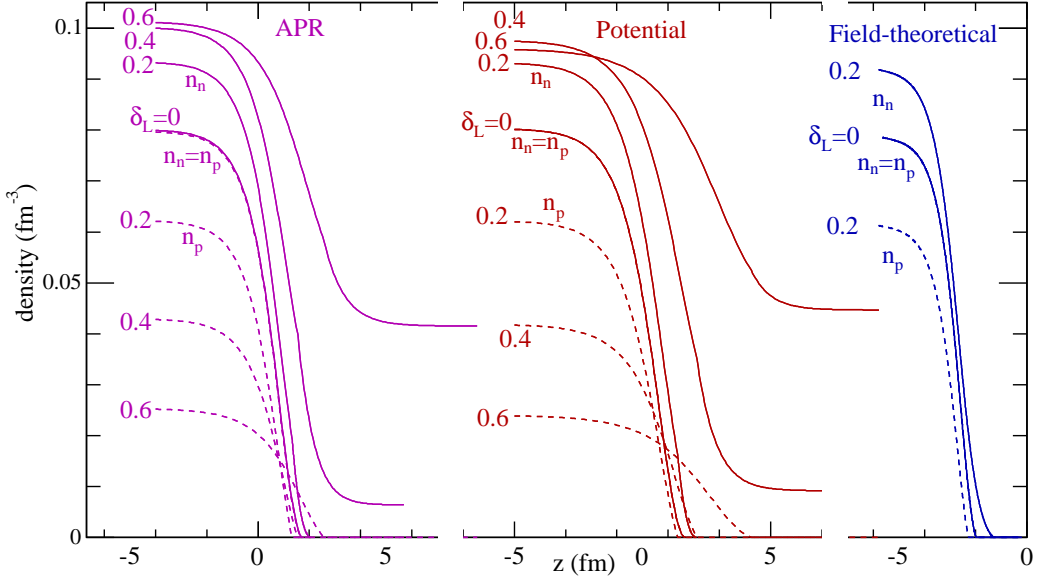


FIG. 5: The semi-infinite matter neutron (solid curves) and proton (dashed curves) density profiles for the indicated values of the asymptotic isospin asymmetry,  $\delta_L$ , as a function of distance  $z$ . The profiles are invariant upon translations along the axis and have been suitably shifted for ease of display. From left to right, results are for the EOS's of the APR, NRAPR, and RAPR models.

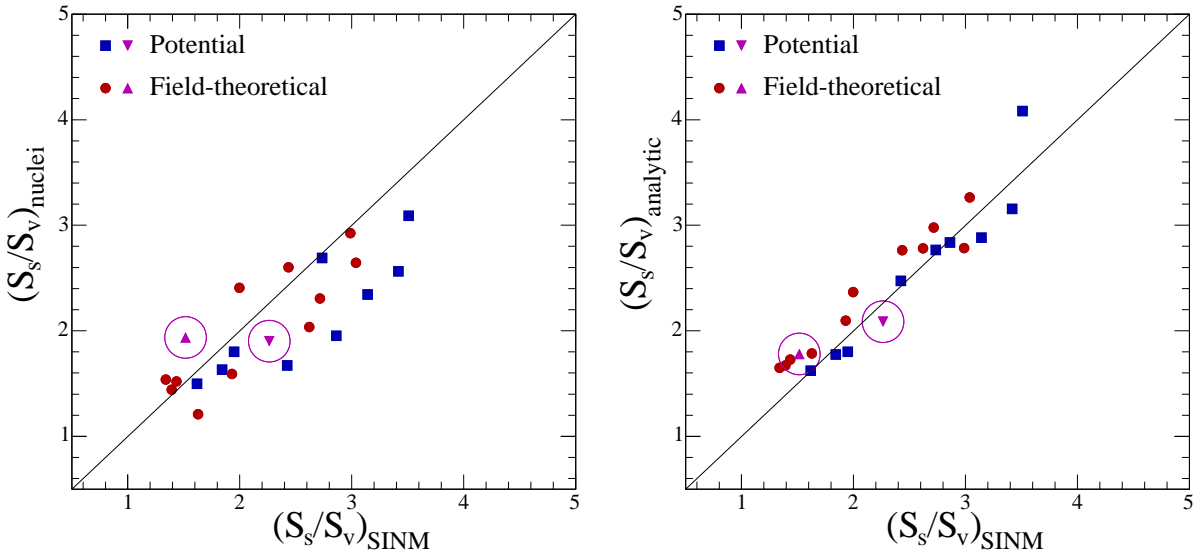


FIG. 6: Left: The ratio of surface to volume contributions,  $S_s/S_v$ , to the total symmetry energy calculated from finite nuclei versus that calculated from semi-infinite matter. Right: The ratio  $S_s/S_v$  calculated from the semi-analytic approximation, Eq. (52), versus that obtained from semi-infinite matter using Eq. (41). In both panels, the downward (upward) triangle is the result for the NRAPR (RAPR) model.

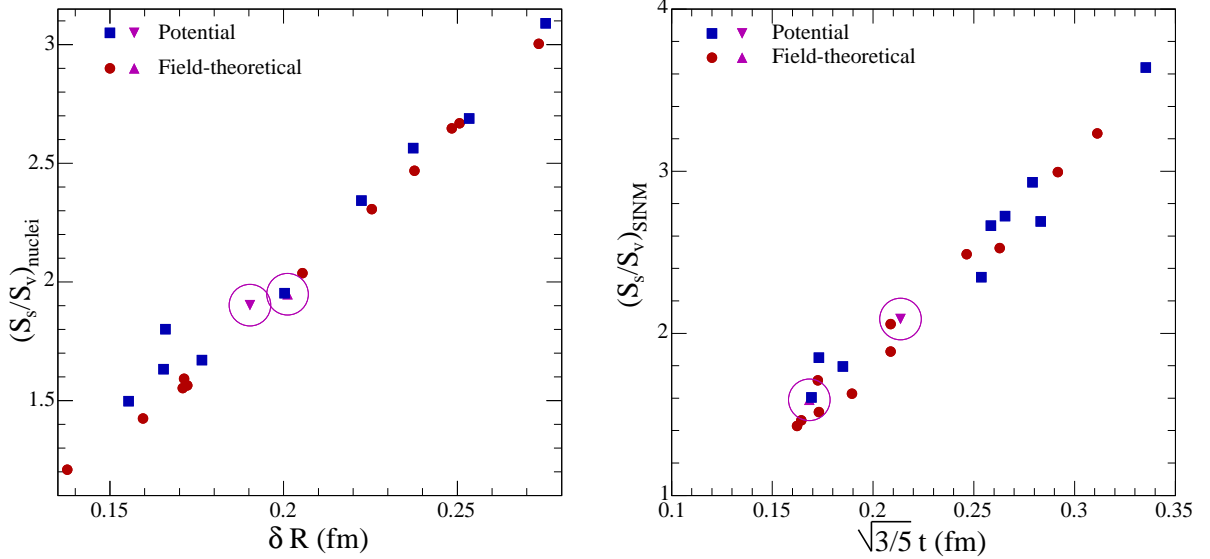


FIG. 7: Correlation between  $S_s/S_v$  and  $\delta R$  derived from nuclei (left panel) and between  $S_s/S_v$  and  $\sqrt{3/5} t$  derived from semi-infinite nuclear matter (right panel).

### B. Semi-infinite matter and finite nuclei

Figure 6 compares different methods of calculating the ratio of the surface to the volume symmetry energy,  $S_s/S_v$ . The left panel shows the values calculated from nuclei using Eq. (78) (with  $\delta_L$  specified by the averaging procedure described earlier) plotted against semi-infinite matter results from Eqs. (41) and (35). The latter values are expected to be the most reliable. The right panel shows the semi-infinite matter results from the approximate relation in Eq. (52) (using, however, exact expressions for the Hamiltonian and the symmetry energy) plotted against the exact semi-infinite results described above. For field-theoretical models, the factor  $\sqrt{Q_{nn} + Q_{np}}$  needed in Eq. (52) is calculated from Eq. (46). In this figure, and in the following figures, potential (field-theoretical) model results are denoted by filled squares (circles). The circled triangles give the APR results from the two fits. There is some scatter about the straight line that indicates perfect agreement between these methods, but the correlation is sufficiently good that it validates the expressions we have used for this ratio. Notice that, apart from the newly constructed SR1, SR2, and SR3 models, the field-theoretical models tend to have a larger value of  $S_s/S_v$  than the non-relativistic models.

In Fig. 7 we display the correlation between  $S_s/S_v$  and the neutron skin thickness  $\delta R$ , or equivalently  $\sqrt{3/5} t$ . In the left panel these quantities are derived from nuclei, whereas for the right panel they are obtained from semi-infinite matter calculations. For the latter, the definition of  $t$  in Eq. (36) is employed with  $\delta_L$  obtained from the lead nucleus (see above). Both panels display a good linear correlation, as suggested by Eq. (54), and the aforementioned tendency of field-theoretical models to have larger values of  $S_s/S_v$  translates into a tendency toward larger values for the skin thickness.

### C. Correlations and Their Origins

In this section, we analyze in some detail the correlations that exist between quantities that are accessible through either laboratory experiments or astronomical observations that shed light on isospin-dependent interactions in nucleonic matter. Our emphasis will be on uncovering the causes of these correlations.

#### 1. Nuclear masses and the correlation between $S_s$ and $S_v$

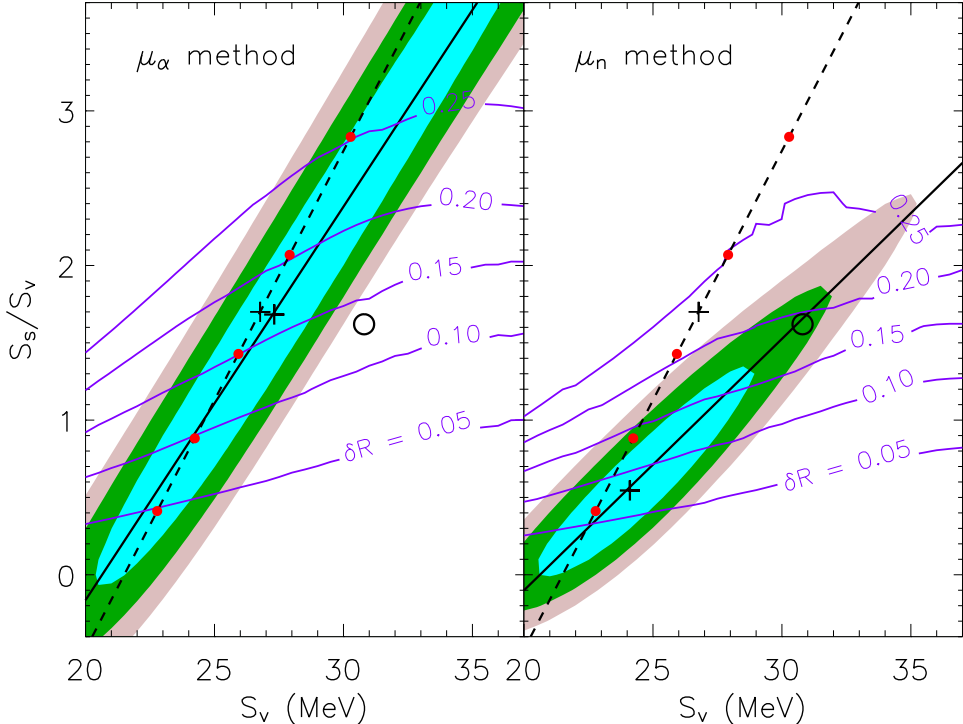


FIG. 8: Correlations in the symmetry energy parameters from liquid droplet fits to nuclear binding energies. The left (right) panel is for the ‘ $\mu_\alpha$ ’ ( $\mu_n$ ) method. Filled-in contours refer to the droplet models that have average errors 0.01, 0.02 and 0.03 MeV/baryon, respectively, above the minimum values (marked by plus signs). The thick solid (dashed) line lies on the minimum  $\chi^2$  valley for our (Danielewicz’s) droplet models. Contours of skin thicknesses ( $\delta R$ ) are shown for our droplet models; corresponding values are indicated on Danielewicz’s correlation with solid dots. The open circles indicate the minimum point found by Møller *et al.* [49].

The formalism for the modified liquid droplet models was discussed in Subsec. III B. Each model has six parameters and we wish to study the correlation between the volume and surface symmetry parameters,  $S_v$  and  $S_s$  (see also Lattimer and Swesty [50]). Therefore as a function of  $S_v$  and  $S_s$ , we have minimized the quantity

$$\chi^2 = \sum_i^n (E_i^D - E_i)^2 / n, \quad (89)$$

with respect to the other four parameters. Here  $E_i^D$  and  $E_i$  are the data [44] and model energies of the  $i$ th nucleus and  $n = 2841$  is the number of nuclei included in the fit (only experimentally determined masses with  $A \geq 20$  are included; the results for a smaller set of nuclei with  $A \geq 40$  are not significantly different). In either case, a nearly linear behavior is found for the contour of minimum  $\chi^2$  between  $S_s/S_v$  and  $S_v$ , as shown in Fig. 8. The equations describing the correlations are given by

$$\begin{aligned} S_s/S_v &= -5.253 + 0.254S_v & \text{for } \mu_\alpha \text{ method,} \\ S_s/S_v &= -3.453 + 0.163S_v & \text{for } \mu_n \text{ method.} \end{aligned} \quad (90)$$

The best-fit values of  $S_v$  and  $S_s/S_v$  are about 27.3 (24.1) MeV and 1.68 (0.545), respectively, for the ‘ $\mu_\alpha$ ’ (‘ $\mu_n$ ’) methods for the modified droplet models.

A relevant question is the range over which values of  $S_v$  and  $S_s$  provide fits that differ by a statistically insignificant amount from the best fit. Traditional mass formula fits were developed to assist in interpolating within or to extrapolate to nearby regimes outside the ranges of measured nuclear masses. The experimental errors of measured masses are of order keV’s per nucleus, so interpolations to the same accuracy are desirable. However, for many astrophysical applications, which involve extrapolations to ranges of  $A$  and  $Z$  well beyond the measured ranges, a model accuracy of a few hundredths of an MeV/baryon would be acceptable. Such an error in the computed energy per particle of a nucleus would translate into a similar error in the neutron or proton chemical potentials. Errors in chemical potentials generated by the use of the “single-nucleus” approximation, an essential assumption of liquid droplet high-density EOS models, are of order  $T/A$  [51], or several hundredths of an MeV, for example.

At the best fit for the droplet models, for which the value of  $\chi^2$  is  $\chi_0^2 \simeq 6$ , the mean difference, or error, between the experimental and predicted nuclear energy per baryon is  $\delta \simeq 0.028$  MeV, where  $\delta$  is defined by

$$\chi_0^2 = \sum_i^n (r_i \delta A_i)^2 / n, \quad (91)$$

and  $r_i$  is a random number between  $-1$  and  $1$ . Therefore, increasing the mean error by a further amount  $\epsilon$  per baryon would increase  $\chi^2$  to a value

$$\chi^2 = \sum_i^n [r_i(\delta + \epsilon) A_i]^2 / n. \quad (92)$$

Contours of mean errors  $\epsilon$  of 0.01, 0.02 and 0.03 MeV per baryon above the minimum are shown in Fig. 8. For the ‘ $\mu_n$ ’ modified droplet model, and for an additional mean error of 0.01 MeV/baryon, the allowable excursions in  $S_v$  are about  $(+5, -4)$  MeV, and in  $S_s/S_v$ , about  $(+0.9, -0.5)$ , even though the excursions must be constrained by the obvious correlation. However, for the ‘ $\mu_\alpha$ ’ model, the allowed excursions in parameters are much larger. It is apparent that fitting nuclear energies alone cannot constrain these parameters, even though a relatively tight correlation between them exists.

The origin of the correlations in Fig. 8 can be most easily understood by examining the functional form of the total symmetry energy in the simple droplet model:

$$E_{sym}(A, I) = S_v A I^2 \left[ 1 + \frac{S_s^*}{S_v A^{1/3}} \right]^{-1}. \quad (93)$$

Assuming that a linear correlation  $S_s^*/S_v = a + bS_v$  exists between the parameters, minimization of Eq. (93) with respect to  $S_v$  yields

$$a = -\left\langle A^{-1/3} \right\rangle^{-1} = -5.31, \quad (94)$$

where the average is mass-weighted over the entire range of nuclear masses used in this study. Noting that

$$\frac{E_{sym}}{A} = \frac{I}{4} \left( \mu_n - \mu_p + 2E_C Z A^{-1/3} + 2E_{dif} Z A^{-1} + \frac{4}{3} E_{ex} Z^{1/3} A^{-4/3} \right), \quad (95)$$

where  $\mu_n - \mu_p$  can be taken directly from nuclear masses as

$$\mu_n - \mu_p \simeq \frac{1}{2} [E(N+1, Z) - E(N-1, Z) - E(Z+1, N) + E(Z-1, N)], \quad (96)$$

one can estimate the average symmetry energy, from which it follows that

$$b = \left\langle I^2 \right\rangle \left\langle \frac{E_{sym}}{A} \right\rangle^{-1} \left\langle A^{-1/3} \right\rangle^{-1} \simeq 0.223. \quad (97)$$

Thus, one has almost precisely the linear relation shown in Eq. (90) for the ‘ $\mu_\alpha$ ’ droplet correlation.

A method similar to the ‘ $\mu_\alpha$ ’ method was suggested by Danielewicz [33]. His results resemble ours, but slight differences in the formulation exist, the most notable being that we account for variation of the central nuclear density in the fitting (*i.e.*, the ratio  $n_L/0.16 \text{ fm}^{-3} \equiv u_0$  in Eqs. (75), (86) and (87)). In addition, Ref. [33] fitted parameters with an absolute energy deviation minimization, rather than the minimization of  $\chi^2$  that we employ. Danielewicz determined best-fit values of  $S_s/S_v \simeq 1.7$  and  $S_v \simeq 27 \text{ MeV}$  and found a correlation slope of 0.32 (compared to 0.25 in our study); Danielewicz’s fit is indicated by the dashed lines in Fig. 8. We have reproduced Danielewicz’s model fits by employing his stated procedures. It is evident that the position of the minimum and the slope of the correlation are affected by differences in the fitting procedure and the droplet formulae. Nevertheless, to within an average error of 0.005 MeV/baryon, the differences found are not significant. Importantly, Ref. [33] found, as do we, that large excursions in parameter space are not excluded within the droplet model. The range of allowed excursions are much smaller for the ‘ $\mu_n$ ’ modified droplet model.

It is interesting that the model of Møller *et al.* [49] gives  $S_v = 30.8 \text{ MeV}$  and  $S_s/S_v = 1.62$ . This point is indicated by a small open circle in the left and right panels of Fig. 8. Clearly it lies much closer to the ‘ $\mu_n$ ’ droplet correlation than the ‘ $\mu_\alpha$ ’ correlation. Although this point is displaced from the position of the best fit for the ‘ $\mu_n$ ’ correlation by over 6 MeV in  $S_v$ , its average error differs from the best fit by less than 0.02 MeV/baryon. In contrast, this point differs by about 0.04 MeV/baryon from the best fit established with the ‘ $\mu_\alpha$ ’ correlation. We note that the model of Ref. [49] contains several additional effects compared to our modified droplet model, including terms representing compression, curvature, deformation and shell effects. It is thus not surprising that the best-fit parameters differ. However, in spite of the fact that the ‘ $\mu_\alpha$ ’ approach contains Coulomb corrections to the surface tension while the ‘ $\mu_n$ ’ approach does not, the notable feature is that the model of Møller *et al.* seems more consistent with the ‘ $\mu_n$ ’ model than the ‘ $\mu_\alpha$ ’ model.

We also compare the volume and surface symmetry coefficients determined for the potential and field-theoretical models developed in this paper with those of the published models utilized here and with the results of mass formula fits to nuclear energies. The parameters of the models developed in this paper have been fit to only four closed shell nuclei, while many of the previously-published forces have been fit to properties of a wider range of nuclei that span a larger range of asymmetries and masses. Thus, we anticipate that a correlation established from mass fits should be apparent when comparing previously-published forces, but not necessarily by the forces developed in this paper. This is precisely what is found, as indicated in Fig. 9. It is important to note that most of the previously-published models follow the correlation of the ‘ $\mu_n$ ’ modified droplet model as opposed to the steeper ‘ $\mu_\alpha$ ’ droplet correlation. This is in spite of the fact that the ‘ $\mu_\alpha$ ’ model takes into account the polarization of the nuclear interior due to Coulomb forces which the ‘ $\mu_n$ ’ model ignores.

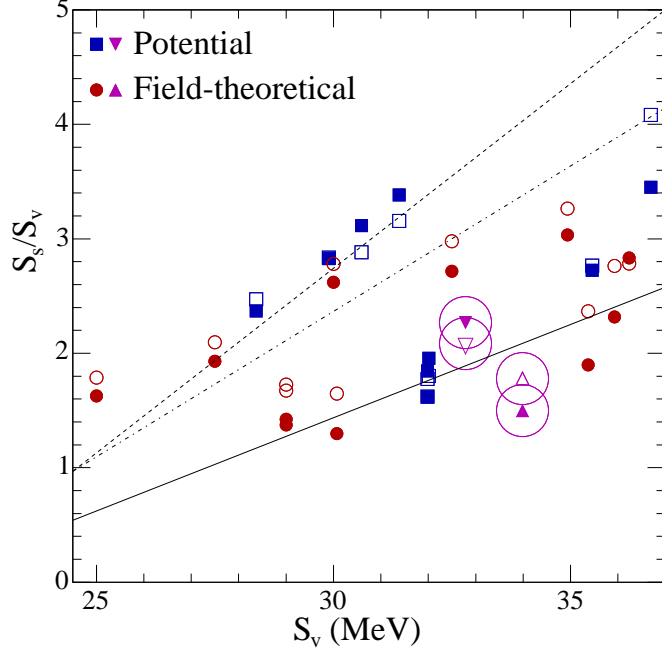


FIG. 9: The ratio of the surface and volume coefficients of the symmetry energy versus the volume coefficient for the models used in this work. The closed symbols show the exact values obtained from a quadratic fit to the surface tension in semi-infinite nuclear matter, whereas the open symbols use the value of  $S_s/S_v$  obtained via Eq. (52). The solid (dot-dashed) line is the linear correlation from the ‘ $\mu_n$ ’ (‘ $\mu_\alpha$ ’) droplet model Eq. (90) and the short-dashed line is the linear correlation from the droplet model of Ref. [33].

These results highlight a major difference between the traditional use of droplet mass formula fits and that of current astrophysical applications. Historically, droplet mass formulae were used to interpolate within known nuclei to establish relatively precise values. In astrophysics, however, it is necessary to extrapolate to extreme conditions of asymmetry. Extrapolations depend significantly upon the correlation between  $S_s/S_v$  and  $S_v$ . Given that the EOS’s in current applications to supernova and neutron star matter are based on a modified droplet approach, it is necessary to use consistent parameter sets obeying the proper correlation. Otherwise, connections between quantities such as the neutron skin thickness and the neutron star radius could be incorrectly interpreted.

Fig. 8 also displays the neutron skin thickness  $\delta R$  as a function of  $S_s$  and  $S_v$  for the two approaches. In the ‘ $\mu_n$ ’ approach, if the dependence upon  $u_0$  were to be ignored, contours of fixed  $\delta R$  would appear as horizontal lines since  $\delta R$  would be a function of  $S_s/S_v$  alone. This would also be the case in the ‘ $\mu_\alpha$ ’ approach, if the dependence upon both  $u_0$  and the Coulomb term  $\beta$  were ignored. The dependence of  $\delta R$  on  $\beta$  is such that  $\partial(\delta R)/\partial S_v < 0$  if the  $u_0$  dependence is ignored, implying a positive slope for the  $\delta R$  contours. Indeed, we find the slope of the  $\delta R$  contours is larger in the ‘ $\mu_\alpha$ ’ approach than in the ‘ $\mu_n$ ’ approach. However, Ref. [33] finds that the  $\delta R$  contours have negative slope; this discrepancy remains to be resolved.

The relationship between the skin thickness and the ratio  $S_s/S_v$  was studied numerically using a variational approach by Bodmer [52]. The results of his work can be understood from our analytical analysis in Section III C. Ref. [52] also emphasizes the interplay between the symmetry and Coulomb energies. Ignoring the latter, as in the ‘ $\mu_n$ ’ method, leads to larger values of  $\delta R$ .

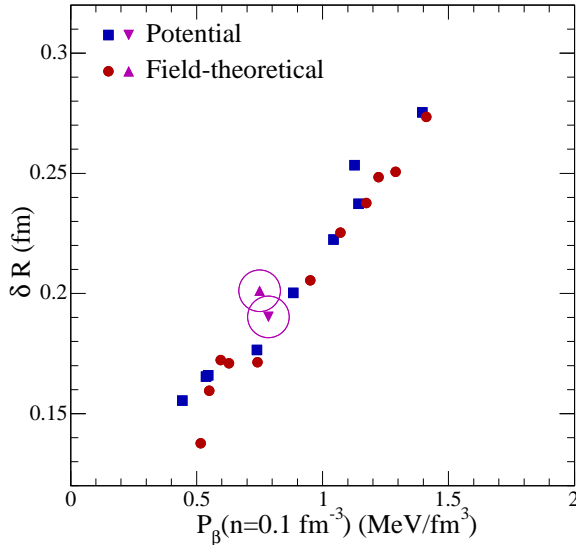


FIG. 10: The neutron skin thickness  $\delta R$  of finite nuclei versus the pressure of  $\beta$ -equilibrated matter at a density of  $0.1 \text{ fm}^{-3}$ .

## 2. The neutron skin thickness versus the pressure of subnuclear neutron-star matter

Typel and Brown [3, 4] have noticed a correlation between the skin thickness and the pressure of pure neutron matter at a density of  $n = 0.1 \text{ fm}^{-3}$ . To the extent that this correlation can be applied, a measurement of  $\delta R$  will help to establish an empirical calibration point for the pressure of neutron star matter at subnuclear densities. Coupled with a neutron star radius measurement (see the discussion below), that could allow the inference of the pressure at supranuclear densities, the Typel-Brown correlation would be valuable in establishing the pressure-density relationship over a wide range of densities inside neutron stars.

The connection between the neutron skin thickness and the symmetry energy has been known from Bodmer's work in the 60's [53]. The Typel-Brown correlation between  $\delta R$  and  $P(5n_0/8)$ , which is closely related to the derivative of the symmetry energy, demonstrates clearly the new information that could be obtained by an accurate measurement of the skin thickness in  $^{208}\text{Pb}$ . Typel and Brown considered a large set of Skyrme parameterizations including those that are inadequate to describe neutron-star matter [40]. Such forces lead to small skin thicknesses. None of the field-theoretical models considered in Ref. [4] yields a skin thickness smaller than 0.2 fm. By using the function  $f$  in Eq. (13), we have constructed examples of field-theoretical models, SR1, SR2, and SR3 which give skin thicknesses which are as small as those obtained from some potential models ( $\sim 0.15 \text{ fm}$ ). Our models es25 and es275 also have small skin thicknesses. However, as pointed out by Furnstahl [54], there are other possible ways in which this could be achieved, including the addition of a  $\delta$  meson or a more complete treatment of pions. If measurements in  $^{208}\text{Pb}$  give  $\delta R \leq 0.15 \text{ fm}$ , then Skyrme-like parameterizations have to be refined at high density to properly describe neutron stars. By the same token, field-theoretical models will need modifications to better describe low-density matter.

We show in Fig. 10 the relation between the skin thickness  $\delta R$  and the pressure of beta equilibrated matter at  $0.1 \text{ fm}^{-3}$ . We have verified that the correlation is similar also at a fixed fraction,  $5/8$ , of the saturation density, for a variety of potential and field-theoretical models.

Some insight into the origin of this correlation can be gained by examining how the beta-equilibrated pressure  $P_\beta$  (the abscissa in Fig. 10) and the neutron skin  $\delta R$  (the ordinate) vary with quantities that depend upon isospin. The pressure of cold, beta-stable neutron-star matter can be written as

$$P_\beta(n, x) = n^2 \left[ E'(n, 1/2) + E'_{sym}(n)(1 - 2x)^2 \right] + P_e + P_\mu, \quad (98)$$

where  $x = n_p/n$  is the proton fraction,  $E(n, 1/2)$  is the energy per particle of symmetric matter,  $E_{sym}(n)$  is the bulk symmetry energy (primes denote derivatives with respect to density), and the last two terms give leptonic (electron and muon) contributions. For beta-equilibrated matter,

$$\begin{aligned} \mu_n - \mu_p &= -\partial E/\partial x \cong 4(1 - 2x)E_{sym}(n) \\ &= \mu_e = \mu_\mu, \end{aligned} \quad (99)$$

where  $\mu_e$  and  $\mu_\mu$  are the chemical potentials of the electron and muon, respectively. This relation, together with the charge neutrality condition,  $n_p = n_e + n_\mu$ , permits the evaluation of the equilibrium proton fraction. Since muons begin to appear in matter for  $n \geq n_0$  [55], the only leptons at subnuclear densities are electrons. The electron pressure is

$$P_e = \frac{1}{4}n_e\mu_e = \frac{1}{4}nx\mu_e \cong nx(1 - 2x)E_{sym}(n), \quad (100)$$

where we have used  $n_e = n_p$  for  $n \leq n_0$  and Eq. (99). Utilizing this relation in Eq. (98), we can write

$$P_\beta(n, x) = P(n, 1/2) + n(1 - 2x)E_{sym}(n) \left[ (1 - 2x) \frac{d \ln E_{sym}(n)}{d \ln n} + x \right], \quad (101)$$

where the first term is the pressure of symmetric nuclear matter. Thus, the total pressure can be written at a particular density in terms of fundamental nuclear parameters. For densities at or below saturation density, the equilibrium proton fraction,  $\tilde{x} \simeq (4E_{sym}/\hbar c)^3/(3\pi^2 n)$ , is very small so that the beta equilibrated pressure and the pure neutron matter pressure only differ by a small amount that depends upon the symmetry properties of the force. Thus, for  $n \leq n_0$ ,  $P_\beta(n) \cong P(n, 1/2) + n^2 E'_{sym}$ , where the second term provides the bulk of the contribution. Thus an approximately linear correlation would result if in Fig. 10  $\delta R$  were plotted against  $E'_{sym}(n)$  at densities  $n = 0.1 \text{ fm}^{-3}$  or  $n = 5n_0/8$ ; such a plot is given in Ref. [56].

The dependence of  $\delta R$  on the isospin asymmetry can be seen explicitly in Eq. (78) for nuclei and in Eq. (54) for the skin thickness of semi-infinite matter. The latter equation can be manipulated to read

$$t = \frac{2\sigma_0}{Bn_L} \frac{\delta_L}{(1 - \delta_L^2)} \lim_{\xi \rightarrow 1} \frac{d}{d\xi} \frac{\int_0^1 u^{1/2} [h_B(u, \delta = 0) + \xi B]^{1/2} [S_v/E_{sym}(u) - 1] du}{\int_0^1 u^{1/2} [h_B(u, \delta = 0) + B]^{1/2} du}, \quad (102)$$

where  $u = n/n_L$  and  $h_B(u, \delta = 0) = \mathcal{H}_B(u, \delta = 0)/n$ . Since  $t \cong \sqrt{5/3} \delta R$ , this relation illustrates that the neutron skin of nuclei is proportional to a specific average of  $[S_v/E_{sym}(u) - 1]$  in the nuclear surface, the averaging function involving the square root of the energy per baryon of isospin symmetric matter.

Equations (98) and (102) show that the density dependence of the symmetry energy is the principal cause of the Typel-Brown correlation. We therefore display the symmetry energies for the models considered in this work in Fig. 11. The thick line indicates the symmetry energy of

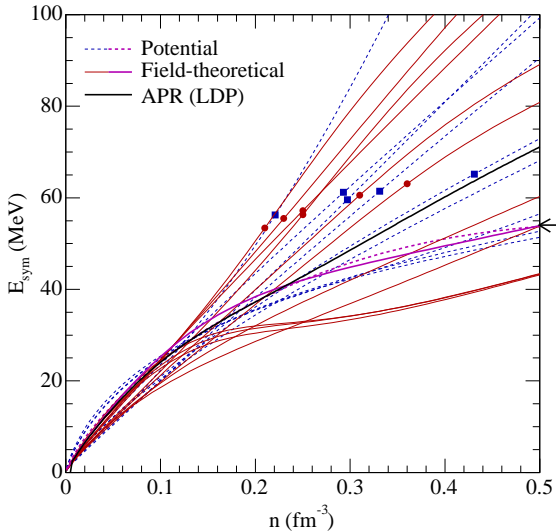


FIG. 11: The symmetry energy versus density for various equations of state. Solid (dashed) lines are for field-theoretical (potential) models. The thick solid line shows the APR symmetry energy for the low density phase. The square (circular) markers indicate the densities at which potential (field-theoretical) models allow the direct Urca process to occur. All models are constrained as discussed in the text. The arrow identifies the NRAPR (dotted line) and RAPR (solid line) models which have nearly identical symmetry energies at  $n = 0.5 \text{ fm}^{-3}$ .

the APR equation of state for the low density phase (this is strictly only applicable for  $n < 0.25 \text{ fm}^{-3}$  for which region the NRAPR and RAPR fits show good agreement). Generally the symmetry energies of the field-theoretical models (solid lines) vary more rapidly with density than those of potential models (dashed lines). Three exceptions, models SR1, SR2, and SR3, were constructed in this work by a suitable choice of the function  $f$  in Eq. (15). These field-theoretical models mimic the density dependence of potential models near the saturation density, but with somewhat different behavior at supranuclear densities. Notice that the requirements that we have placed on our models strongly constrain the symmetry energy at an average nuclear density  $n \simeq 0.1 \text{ fm}^{-3}$ , in agreement with Brown [3] and Horowitz and Piekarewicz [7] (see also Ref. [54]).

For the models considered in Fig. 11, the variation of  $\delta R$  with  $P_\beta$  shown in Fig. 10 confirms the Typel-Brown correlation. Additional points that emerge from our analysis include:

- (1) At the densities of interest, the pressure difference between pure neutron matter and beta-equilibrated matter is small enough that the correlation is not significantly impacted.
- (2) In general, field-theoretical models yield  $\delta R > 0.2 \text{ fm}$ . The exceptions are models SR1, SR2, SR3, es25, and es275 that were designed to have special symmetry properties that lead to  $\delta R < 0.2 \text{ fm}$ .
- (3) If the neutron skin thickness is measured with high accuracy, the pressure of neutron-star matter at this density could be determined to within (20–25)%. For a fiducial  $R_n - R_p = 0.2 \pm 0.025 \text{ fm}$ , this correlation predicts that  $P_\beta = (0.9 \pm 0.3) \text{ MeV/fm}^3$ ; for a lower mean value of  $R_n - R_p$ , the predicted uncertainty in the pressure is larger. Employing a wider variety of non-relativistic models than those used by Typel and Brown results in an enlarged spread in results for models with relatively small values of  $\delta R$ . We emphasize that the linear correlations observed in Fig. 10 are significantly worsened for slight excursions from the fiducial densities chosen.

Furnstahl [54] has presented a correlation between the neutron form factor and the neutron

radius. He also demonstrated correlations between the skin thickness and, separately, the linear density dependence of the symmetry energy, the quadratic density dependence and also  $d^2n_0/d\alpha^2$ . These three quantities are all closely related to  $P(5n_0/8)$  as shown above.

*Implications for neutrino emission from neutron stars*

The density dependence of the symmetry energy also plays an important role in determining whether or not the simplest possible  $\nu$  emitting processes, the so-called direct Urca processes

$$p + \ell \rightarrow n + \nu_\ell \quad \text{and} \quad n \rightarrow p + \ell + \bar{\nu}_\ell, \quad (103)$$

where  $\ell$  is either an electron or a muon, occur in charge neutral neutron star matter. These direct Urca processes can occur whenever energy and momentum conservation is simultaneously satisfied among  $n$ ,  $p$  and  $\ell$  (for temperatures of interest to long-term cooling, neutrinos would have left the star). In a mixture of neutrons, protons and electrons, the required proton fraction  $x$  for the direct Urca process to occur is 1/9. When this mixture is in beta equilibrium,  $x$  satisfies [50]

$$x \simeq 0.048 (E_{sym}(n)/S_v)^3 (n_0/n) (1 - 2x)^3, \quad (104)$$

which highlights the role of the density dependent symmetry energy. For example, for a linear symmetry energy,  $E_{sym}(n) = S_v(n/n_0)$ , the onset of the direct Urca process occurs for  $n_c/n_0 \simeq 2.2$  with  $S_v = 30$  MeV. In the presence of muons, which begin to appear around  $n_0$ , the required proton fraction is about 0.14 and hence the threshold density is somewhat larger. In the case that  $E_{sym}(n)$  increases less than linearly with density, the direct Urca threshold density is larger. If the Urca threshold density is less than the star's central density, the neutron star will rapidly cool because of large energy losses due to neutrino emission: the star's interior temperature  $T$  will drop below  $10^9$  K in minutes and reach  $10^7$  K in about a hundred years. This is the so-called rapid cooling paradigm. If the threshold density is not reached below the central density, or if the direct Urca process is suppressed due to nucleon superfluidity (calculated energy gaps are about an MeV or less), cooling instead proceeds through the significantly less rapid modified Urca processes

$$n + (n, p) \rightarrow p + (n, p) + e^- + \bar{\nu}_e \quad \text{and} \quad p + (n, p) \rightarrow n + (n, p) + e^+ + \nu_e, \quad (105)$$

in which an additional nucleon enables momentum conservation. As the temperature approaches the superfluid critical temperature, cooling also takes place through neutrino pair emission from the Cooper-pair breaking and formation processes [57] which are more efficient than the modified Urca process, but significantly less efficient than the direct Urca process. If the density dependence of the nuclear symmetry energy is relatively weak, only the less rapid neutrino cooling processes can occur.

The filled squares and circles in Fig. 11 indicate the densities at which the direct Urca process is allowed by energy and momentum conservation conditions. Some of the models whose symmetry energy exhibits a moderate density dependence allow the direct Urca process to take place, but at densities beyond the maximum of  $0.5 \text{ fm}^{-3}$  plotted. For some other models the direct Urca process does not occur at all since it requires densities larger than the central densities of the maximum mass stars.

Figure 12 shows the skin thickness versus the threshold density for the direct Urca process (note that the NRAPR and RAPR skin thicknesses are plotted against  $n_{Urca}$  for the exact APR EOS.). The results in this figure supplement those of Horowitz and Piekarewicz [58] by also including results of potential models. A determination that  $\delta R$  has a value greater than 0.2 fm would imply that the nucleon direct Urca process should exist in  $1.4 \text{ M}_\odot$  neutron stars, unless it is suppressed

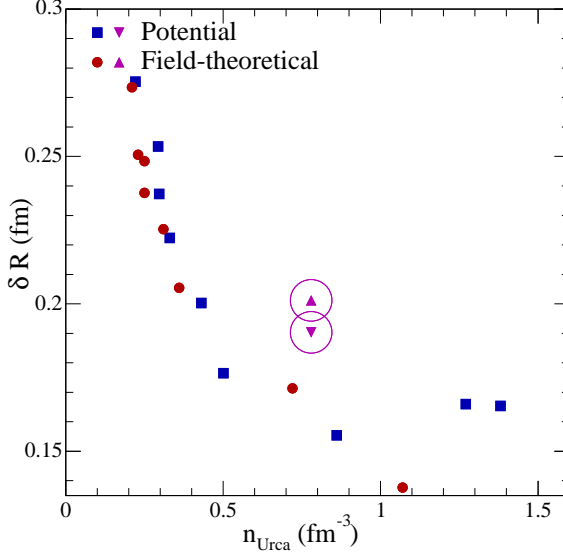


FIG. 12: Skin thickness versus the threshold density for the direct Urca process to occur in neutron stars.

by superfluidity. For a recent assessment in this regard, see Ref. [59] which studied neutron star cooling in the absence of enhanced neutrino emission, and compared the results with data on cooling neutron stars.

#### *Implications for the crustal fraction of the moment of inertia*

Another astrophysical application concerns the thickness of the crust of a neutron star, which is related to the density dependence of the symmetry energy by physics similar to that of the thickness of the neutron skin of nuclei. The neutron star crust thickness might be measurable from observations of pulsar glitches, the occasional disruptions of the otherwise extremely regular pulsations from magnetized, rotating neutron stars. The canonical model of Link et al. [60] suggests that glitches are due to the transfer of angular momentum from superfluid neutrons to normal matter in the neutron star crust, the region of the star containing nuclei and nucleons that have dripped out of nuclei. This region is bounded by the neutron drip density ( $\simeq 1.5 \times 10^{-3} n_0 \simeq 4 \times 10^{11} \text{ g cm}^{-3}$ ) and the transition density  $n_t$  ( $\approx n_0/2 \simeq 1.5 \times 10^{14} \text{ g cm}^{-3}$ ) at which nuclei merge into uniform nucleonic matter. Link et al. [60] concluded from glitches of the Vela pulsar that at least 1.4% of the total moment of inertia resides in the crust of the Vela pulsar. The fraction of the star's moment of inertia contained in the crust is connected to the crust's thickness, and both are controlled by the pressure of matter,  $P_t$ , at the transition density as well as the neutron star's mass  $M$  and radius  $R$ . The fractional moment of inertia,  $\Delta I/I$ , where  $\Delta I$  is the moment of inertia in the star's crust and  $I$  is the star's total moment of inertia, can be expressed as [2] :

$$\frac{\Delta I}{I} \simeq \frac{28\pi P_t R^4}{3GM^2} \frac{(1 - 1.67\beta - 0.6\beta^2)}{\beta} \left[ 1 + \frac{2P_t(1 + 5\beta - 14\beta^2)}{n_t m_b c^2 \beta^2} \right]^{-1}, \quad (106)$$

where  $\beta = GM/Rc^2$ .

The core-crust transition density is not too far from  $0.1 \text{ fm}^{-3}$ , and matter at these densities is nearly pure neutron matter, which suggests that the Typel-Brown correlation between  $n_t$  and  $\delta R$

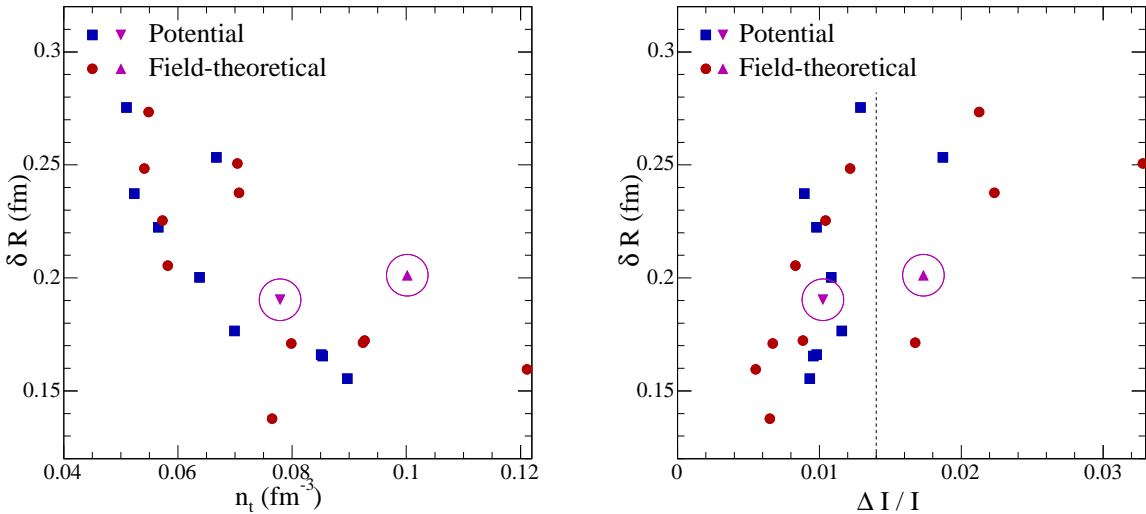


FIG. 13: Neutron skin thickness versus the core-crust interface density  $n_t$  (left panel) and the fractional moment of inertia  $\Delta I/I$  in the crust of a  $1.4M_\odot$  neutron star (right panel). The dashed line for  $\Delta I/I = 0.014$  is deduced for the Vela pulsar, assuming a mass for Vela of  $1.4M_\odot$ .

has astrophysical significance. However, the Typel-Brown correlation refers to the fiducial density,  $0.1 \text{ fm}^{-3}$ . Thus, even if the transition density was always  $0.1 \text{ fm}^{-3}$ , the dependence of  $R$  (for a given  $M$ ) on the symmetry energy has to be taken into account also. The major dependence on the EOS is therefore through the quantity  $P_t R^4/M^2$ .

A reasonable approximation to the core-crust boundary can be obtained by considering the zero temperature phase equilibrium between two homogenous nucleonic fluids, a dense phase approximating matter inside nuclei (labelled by  $i$ ) and a dilute phase approximating the drip nucleons outside nuclei (labelled  $o$ ). Finite-size effects, such as those due to the surface and Coulomb energy can be included as in Ref. [61], but are ignored here to obtain a first orientation. The electrons can be treated as a free Fermi gas which uniformly fills space in both phases and we define  $Y_e$  to be the ratio of electron and baryon densities.

Phase equilibrium follows from minimization of the free energy density allowing for the two conserved quantities of baryon number and charge. We define  $u$  to be the fractional volume occupied by the dense phase  $i$ . The dense phase  $i$  has a proton fraction  $x_i$ ; the dilute phase  $o$  has a proton fraction  $x_o$ . Phase equilibrium, while maintaining beta equilibrium, is then described by

$$\begin{aligned} n &= n_i u + n_o (1 - u), & n Y_e &= n_i x_i u + n_o x_o (1 - u), & P_i &= P_o, \\ \mu_{ni} &= \mu_{no} & \mu_{pi} &= \mu_{po}, & \mu_{ni} - \mu_{pi} &= \mu_e. \end{aligned} \quad (107)$$

The transition density occurs at the baryon density  $n = n_t$  for which  $u \rightarrow 0$ .

Figure 13 displays the relation between  $\delta R$  and  $n_t$  (left panel) and the relation between  $\delta R$  and  $\Delta I/I$  (right panel) for a  $1.4 M_\odot$  star. The transition density varies over a range of about a factor of 2 in density, from  $0.05 \text{ fm}^{-3}$  to  $0.12 \text{ fm}^{-3}$ , and there is a negative correlation between  $\delta R$  and  $n_t$ , but it is not very robust when all the models are considered. We note that Horowitz and Piekarewicz [7] computed the transition density as the density at which an instability to small perturbations occurs in a uniform liquid of nucleons and electrons (see also Ref. [25]). They obtained a much tighter correlation between  $n_t$  and  $\delta R$  by varying the symmetry energy in a few relativistic models. Using

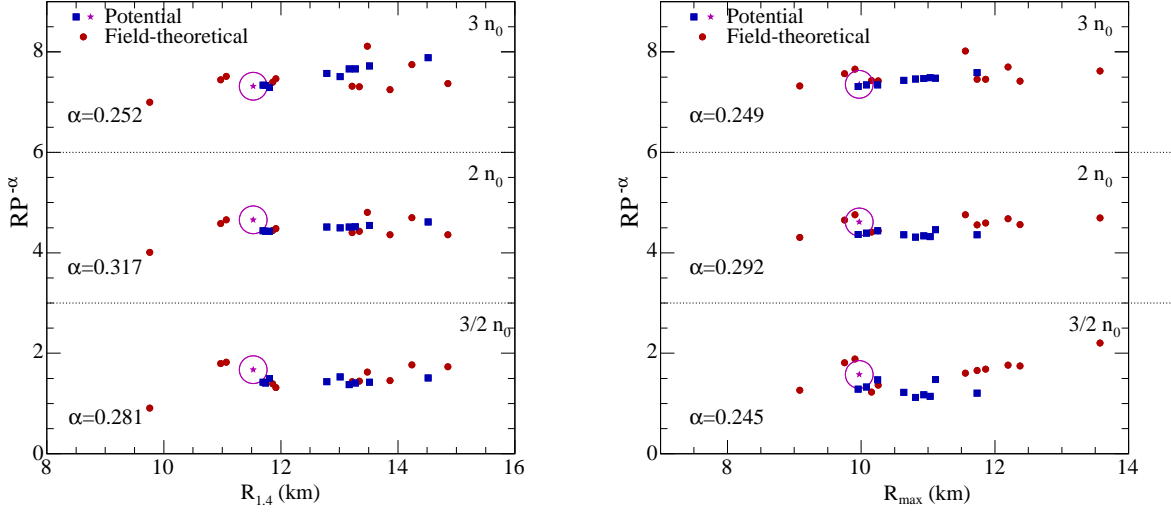


FIG. 14: The quantity  $RP^{-\alpha}$  as a function of the stellar radius  $R$ , for pressures  $P$  determined at  $3/2$ ,  $2$  and  $3$  times equilibrium nuclear matter density. For each density, the best-fit value for the exponent  $\alpha$  is as indicated. Results for  $1.4M_{\odot}$  (maximum mass) stars are in the left (right) panel. Circled stars indicate the results obtained with the APR equation of state.

the exact APR EOS our method yields  $n_t = 0.094 \text{ fm}^{-3}$  in close agreement with Ref. [25]; this lies between the RAPR and NRAPR results plotted in Fig. 13 being somewhat closer to the former.

Although we do not display it, there is little correlation between  $P_t$  and  $\delta R$ . One would expect high values of  $S'_v$  to correspond to high pressures in general. However, high values of  $S'_v$  also tend to have low transition densities, so the effects somewhat cancel, leaving little net correlation between  $P_t$  and  $S'_v$ . However, as discussed above, the astrophysical observable  $\Delta I/I$  is nearly proportional to the quantity  $P_t R^4/M^2$  and not  $P_t$  alone. This is plotted in the right panel in Fig. 13. Although the correlation is not very strong, it does suggest that, at least in the case of a  $1.4M_{\odot}$  Vela pulsar, a value of  $\Delta I/I \sim 0.014$  implies a skin thickness  $> 0.15 \text{ fm}$  for  $^{208}\text{Pb}$ . A larger mass for the Vela relaxes this lower bound toward lower values of  $\delta R$ .

### 3. The neutron star radius versus the pressure of supranuclear neutron-star matter

Lattimer and Prakash [2] found that the radius  $R$  of a neutron star exhibits a correlation that has the form of a power law:

$$R \simeq C(n, M) [P(n)]^{0.23-0.26}, \quad (108)$$

where  $P(n)$  is the total pressure inclusive of leptonic contributions evaluated at a density  $n$  in the range  $1$  to  $2n_0$ , and  $C(n, M)$  is a number that depends on the density  $n$  at which the pressure was evaluated and on the stellar mass  $M$ . In Fig. 14 the left and right panels show this correlation as  $RP^{-\alpha}$  versus  $R$  for stars of mass  $1.4M_{\odot}$  and  $M_{max}$ , respectively, for the EOS's considered here and densities  $n = 1.5 - 3n_0$ . In each case, the exponent  $\alpha$  was determined by a least-squares analysis to give the best correlation. For the optimum exponent  $\alpha = d \ln R / d \ln P \sim 0.25$ , the radius increases very slowly with mass. As shown in Ref. [2], general relativity reduces the value of  $\alpha$  from  $1/2$ , the

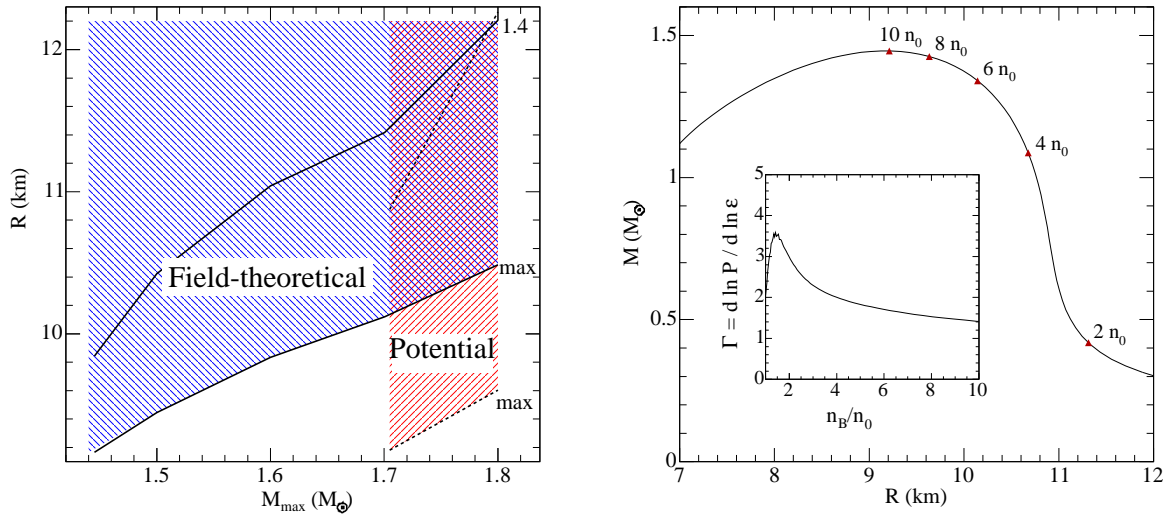


FIG. 15: Left panel: The smallest radii of neutron stars given by our set of EOS's as a function of the corresponding maximum masses for field-theoretical and Skyrme models (respectively, solid and dashed lines labelled “max”). The radii for  $1.4M_{\odot}$  neutron stars are labelled “1.4”. The shaded regions indicate radii that are accessible for a particular class of EOS. Right panel: The mass–radius relation for the field-theoretical model SR1. The central densities of stars of different masses are as indicated. The inset shows the adiabatic index  $\Gamma$  versus density for this model.

value characteristic of an  $n = 1$  Newtonian polytrope. For the EOS of Buchdahl [62], this role of general relativity was demonstrated analytically [2].

In studying the Lattimer-Prakash radius-pressure correlation [2], we have excluded cases in which the high density EOS was softened because of the presence of non-nucleonic degrees of freedom. The correlation, however, is not greatly improved by this omission, primarily because softening components do not often affect the equation of state strongly until the density exceeds two to three times the saturation density.

The discussion in Sec. IV C 2 showed that the pressure at densities close to equilibrium density is dominated by the derivative of the symmetry energy. Thus one could alternatively achieve a linear correlation by plotting  $E'_{sym}(3n_0/2)$  versus  $R^{1/\alpha}$ .

#### *Sizes of neutron star radii in potential and field-theoretical models*

We have not considered in this work the possible presence of hyperons, Bose (pion or kaon) condensates or quarks. Such components generally soften the EOS which results in neutron stars with masses and radii that are smaller than those with nucleons-only matter. Our interest here lies in establishing the minimum radii that EOS's with only nucleonic matter yield. Fig. 15 displays this minimum radius as a function of maximum mass for potential and field-theoretical EOS's that are constrained as described in Sec. IV A.

Each point on the solid line labeled “max” is the radius of the maximum mass configuration for the field-theoretical EOS which yields the smallest possible radius. The solid line labeled “1.4” is the radius of a  $1.4M_{\odot}$  star for the same EOS. Analogous results for potential models are shown by the dashed lines. The hatched regions indicate where other reasonable potential or field-theoretical

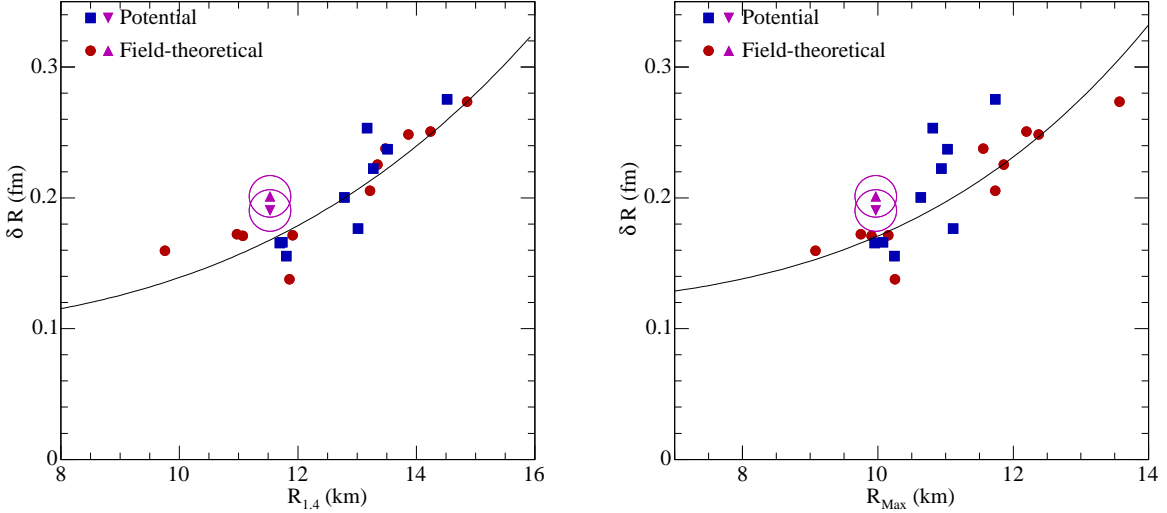


FIG. 16: Calculated neutron skin thickness  $\delta R$  of nuclei versus the radius of  $1.4M_{\odot}$  stars (left panel) and of maximum mass stars (right panel). The solid lines are described in the text.

models may exist. For comparison, the APR equation of state supports a star of maximum mass  $2.2M_{\odot}$  for which the radius is 10.9 km. The field-theoretical models SR1, SR2, and SR3 have maximum masses of  $1.44$ ,  $1.6$ , and  $1.8 M_{\odot}$ , respectively. The corresponding radii are

$$\begin{aligned} R_{1.4} &= 9.84, 11.04, \text{ and } 12.21 \text{ km} & \text{for } M = 1.4M_{\odot} \\ R_{max} &= 9.17, 9.83, \text{ and } 10.49 \text{ km} & \text{for } M = M_{max}. \end{aligned} \quad (109)$$

The mass-radius relation of the model SR1 with a maximum mass of  $1.44 M_{\odot}$  is shown in the right panel of Fig. 15. Of the many field-theoretical models considered in this work, this model yields the smallest radius.

#### 4. The neutron skin thickness versus the neutron star radius

We turn now to the Horowitz-Piekarewicz correlation for the models considered in this work. Our results are shown in Fig. 16 for a  $1.4M_{\odot}$  (left panel) and for the maximum mass (right panel) configuration for each EOS. Note especially the results of models SR1, SR2, and SR3 which buck the trend of field-theoretical models that generally yield large neutron star radii. As noted in Ref. [2], large radii are a consequence of symmetry energies that vary rapidly with density beyond the nuclear saturation density.

The Typel-Brown correlation demonstrates that the neutron skin thickness  $\delta R$  is linearly correlated with  $E'_{sym}(5n_0/8)$ , whereas the Lattimer-Prakash correlation for the neutron star radius establishes a linear correlation between  $R^{1/\alpha}$  and  $E'_{sym}(3n_0/2)$ . These two correlations can be synthesized by comparing  $E'_{sym}$  at the two different densities. This is carried out in Fig. 17 where, notwithstanding some scatter in the results, there is an overall linear correlation between  $E'_{sym}(5n_0/8)$  and  $E'_{sym}(3n_0/2)$ . This suggests a relationship of the form  $\delta R = a + bR^{1/\alpha}$ . Determining the coefficients by a least-squares fit to the results in Fig. 16 yields

$$\delta R = \left( 0.09558 + 1.201 \times 10^{-5} R^{1/0.281} \right) \text{ fm} \quad \text{for } M = 1.4M_{\odot}$$

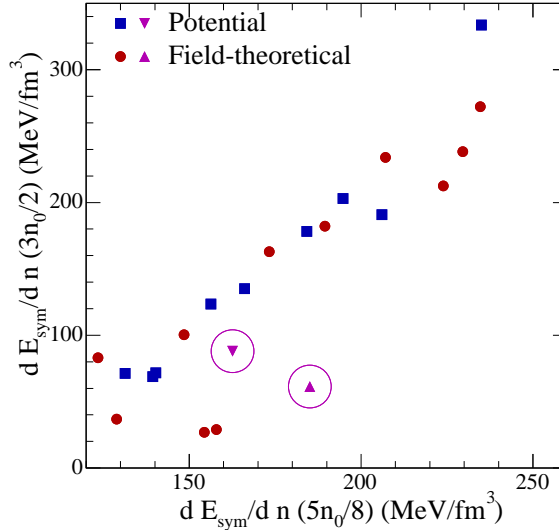


FIG. 17: The derivative of the symmetry energy at  $3n_0/2$  versus that at  $5n_0/8$ .

$$\delta R = \left( 0.1160 + 4.540 \times 10^{-6} R^{1/0.245} \right) \text{ fm} \quad \text{for } M = M_{max}, \quad (110)$$

These relationships are depicted by solid lines in Fig. 16. For a fiducial  $\delta R = 0.2 \pm 0.025$  fm,  $R_{1.4} = (13 \pm 0.5)$  km and  $R_{max} = (11 \pm 0.5)$  km. In the latter case,  $M_{max}$  is found to vary up to  $2.2M_\odot$ . These values give a measure of the extent to which the neutron star radius can be constrained if the neutron skin thickness is measured to the specified accuracy. For a lower mean value of  $\delta R$  the uncertainty in the radius is larger.

Schramm [63] further explored the Horowitz-Piekarewicz correlation [7, 64] between the neutron skin thickness and the neutron star radius by using covariant field-theoretical models based on SU(3) symmetry. He found that the correlation was weak because of the restricted variation allowed in the fourth-order vector-isovector couplings. In our work we have eliminated EOS's which do not satisfy minimal astrophysical and experimental nuclear constraints, which results in a tight correlation despite the enlarged freedom in the description of the symmetry energy. In fact, combining the correlations as discussed above, we find a skin thickness which scales approximately with the stellar radius raised to a power  $\sim 4$ .

## V. OTHER RELATED CORRELATIONS

We turn now to address a few other correlations connected with isospin asymmetry. Supplements to our brief account here are contained in several reviews, some of which are alluded to below.

### A. Giant Dipole Resonances

The analyses of giant resonances, particularly dipole resonances, have long served to delineate the role of volume and surface effects in nuclei; for a review see Ref. [65]. In medium to heavy nuclei in which magnetic contributions are small, the inverse-energy-squared weighted photoabsorption

cross section can be related to the static polarizability  $p$  as

$$\sigma_{-2} = \int \frac{\sigma(\omega)}{\omega^2} d\omega = 2\pi^2 (e^2/\hbar c) p. \quad (111)$$

In nuclei with mass number  $A \geq 100$ ,  $\sigma_{-2} = (2.9 \pm 0.2) A^{5/3} \mu\text{b MeV}^{-1}$  parameterizes the data [66, 67]. The dipole polarizability can be evaluated as the response of a nucleus to an external dipole field  $\eta D$ , where  $\eta$  denotes the strength and  $D = (1/2) \sum_{i=1}^A z_i \tau_i^3$  is the dipole operator. Explicitly,

$$p = 2 \sum_{n \neq 0} \frac{|\langle 0 | D | n \rangle|^2}{\omega_n - \omega_0}, \quad (112)$$

where  $|n\rangle$  and  $\omega_n$  are the eigenstates and eigenenergies of the nuclear Hamiltonian responsive to the dipole operator  $D$ . Microscopic RPA calculations [68] of  $p$  employing Skyrme-like interactions reproduce the general trends of the data. The interplay between volume and surface effects are, however, difficult to extract from RPA calculations. Semiclassical methods, in which the energy density formalism is coupled with a hydrodynamic approach to describe collective excitations, have thus been employed to explore how the volume and surface symmetry energies,  $S_v$  and  $S_s$ , determine the value of  $p$  across the periodic table [31, 65, 69]. Using the Hamiltonian density in Eq. (1), and writing the transition density as  $\delta[\rho_n(r) - \rho_p(r)] = \eta\phi(r) \cos\theta$ , the polarizability is calculated from

$$p = \frac{2\pi}{3} \int \phi(r) r^3 dr, \quad (113)$$

where  $\phi(r)$  is the solution of the corresponding Euler-Lagrange (integro-differential) equation. It is found that similar results for  $p$  are obtained for correlated values of  $S_v$  and  $S_s$ . Numerical results for  $^{40}\text{Ca}$ ,  $^{120}\text{Sn}$ , and  $^{208}\text{Pb}$  show that the choice of  $S_v$  in the range 27–42 MeV requires  $|S_s/S_v| = 1.2\text{--}2.2$ ; lower values of  $S_v$  correlate with lower values of  $S_s$  for good fits [69]. The slope of this correlation can be compared to that found using ground state energetics in Sec. IV C 1 (see Fig. 8). It is in close agreement with the correlation obtained with the ‘ $\mu_n$ ’ model.

A qualitative understanding of this correlation can be gained by using a schematic symmetry energy density functional and a leptodermous expansion of the density [65], whence one obtains the result

$$p = \frac{A \langle r^2 \rangle}{24 S_v} \left( 1 + \frac{5}{3} \frac{S_s}{S_v} A^{-1/3} + \dots \right), \quad (114)$$

where  $\langle r^2 \rangle$  is the mean square radius of the nucleus and higher order terms contain corrections from the diffuseness and the skin thickness. Although values of  $S_v = 32.5$  MeV and  $|S_s/S_v| = 2.2$  describe the data adequately [65], correlated variations in these numbers are allowed as pointed out in Ref. [69].

Sum rules have been particularly useful to relate experiments and theory in discussing the mean excitation energies, widths, and the spreading of the excitation strengths [65]. The moments  $m_p$  of the strength function  $S(\omega) = \sum_{n>0} |\langle n | F | 0 \rangle|^2 \delta(\omega - \omega_n)$  defined by

$$m_p = \int_0^\infty S(\omega) \omega^p d\omega = \sum_{n>0} |\langle n | F | 0 \rangle|^2 \omega_n^p, \quad (115)$$

where  $F$  is the physical operator exciting the nucleus from its ground state  $|0\rangle$  to its eigenstate  $|n\rangle$ , are especially helpful in this regard. For example, a good measure of the mean excitation energy is provided by  $E(D) = \sqrt{m_1/m_{-1}}$ , for which results from RPA and hydrodynamic calculations have

been compared with data [65]. Using a droplet model coupled with a hydrodynamic approach to excite the dipole resonance, Ref. [70] obtains

$$E(D) = \sqrt{\frac{6\hbar^2(1+K_D)}{M\langle r^2 \rangle} \frac{S_v}{1 + \frac{5}{3} \frac{S_s}{S_v} A^{-1/3}}}, \quad (116)$$

where  $M$  is the nucleon mass. The quantity  $K_D$  is a model dependent enhancement factor characterizing the relative contribution of the nuclear interaction to the  $m_1$  sum rule and depends critically on the value of the energy up to which the energy integration is carried out in analyzing the experimental data. Using values of  $S_v = 32.5$  MeV and  $S_s/S_v \simeq 2$  from a droplet model fit to nuclear energies, and  $K_D = 0.2$  corresponding to  $E_{max} = 30$  MeV, Ref. [70] finds that a hydrodynamic approach is able to reproduce the experimental mean excitation energy of nuclei ranging from  $^{40}\text{Ca}$  to  $^{208}\text{Pb}$  reasonably well. Several Skyrme interactions with different values of  $S_v$  and  $S_s/S_v$  are also able to account for the data to the same level of accuracy. However, since the values of  $S_v$  and  $S_s$  for these forces are correlated because they are fit to experimental masses, the additional constraint on the permitted ranges of  $S_v$  and  $S_s$  resulting from fitting dipole resonances does not seem to be significant.

It must be emphasized that while a hydrodynamic approach is able to account for the gross features of nuclear mass dependence, several detailed features of the data such as strength fractionation, spreading widths, etc., are not naturally incorporated in its scope. For such details one must adopt a more microscopic approach that includes, for example, contributions from 2p–2h excitations, etc. For a detailed account, see, for example, Ref. [71].

## B. Heavy-Ion Collisions

### 1. Multi-fragmentation

The breakup of excited nuclei into several smaller fragments during an intermediate-energy heavy-ion collision probes the phase diagram of nucleonic matter at sub-saturation density and moderate ( $\sim 10 - 20$  MeV) temperatures. In this region of the phase diagram the system is mechanically unstable if  $(dP/dn)_{T,x} < 0$ , and/or chemically unstable if  $(d\mu_p/dx)_{T,P} < 0$ . (A pedagogical account of such instabilities can be found in Ref. [72]). These instabilities, which are directly related to the symmetry energy at sub-saturation densities [73], are believed to trigger the onset of multifragmentation. Because of the instabilities, matter separates into coexisting liquid and gas phases, which each have different proton fractions, *i.e.* “isospin fractionation” [74]. This fractionation is observed in the isotopic yields which can potentially reveal information about the symmetry energy. Also, the scaling behavior of ratios of isotope yields measured in separate nuclear reactions, “isoscaling”, is sensitive to the symmetry energy [75, 76]. This scaling is expressed in the empirically observed ratio of fragment yields from two similar systems with different neutron-to-proton ratios:

$$Y_2(N, Z)/Y_1(N, Z) \sim \exp^{\alpha N + \beta Z}, \quad (117)$$

where the constants  $\alpha$  and  $\beta$  can be related to the neutron and proton chemical potentials in a canonical ensemble description, and thus to the proton fraction of the source. To date, there are many suggestions of how the symmetry energy may affect multifragmentation [77]. Ongoing research is concerned with an extraction of reliable constraints on the symmetry energy from the presently available experimental information.

## 2. Collective Flow

Nuclear collisions in the range  $E_{lab}/A = 0.5 - 2$  GeV offer the possibility of pinning down the equation of state of matter above normal nuclear density (up to  $\sim 2$  to  $3n_0$ ) from a study of matter, momentum, and energy flow of nucleons [78]. The observables confronted with theoretical analyses include (i) the mean transverse momentum per nucleon  $\langle p_x \rangle/A$  versus rapidity  $y/y_{proj}$  [79], (ii) flow angle from a sphericity analysis [80], (iii) azimuthal distributions [81], and (iv) radial flow [82]. Flow data gathered to date are largely for protons (as detection of neutrons is more difficult) and for collisions of laboratory nuclei in which the isospin asymmetry is not large. Theoretical calculations have generally been performed using Boltzmann-type kinetic equations. One such equation for the time evolution of the phase space distribution function  $f(\vec{r}, \vec{p}, t)$  of a nucleon that incorporates both the mean field  $U$  and a collision term with Pauli blocking of final states is (see, for example, Ref. [83])

$$\frac{\partial f}{\partial t} + \vec{\nabla}_p U \cdot \vec{\nabla}_r f - \vec{\nabla}_r U \cdot \vec{\nabla}_p f = - \frac{1}{(2\pi)^6} \int d^3 p_2 d^3 p_{2'} d\Omega \frac{d\sigma_{NN}}{d\Omega} v_{12} (2\pi)^3 \delta^3(\vec{p} + \vec{p}_2 - \vec{p}'_1 - \vec{p}'_2) \times [f f_2 (1 - f_1) (1 - f_2) - f_1 f_2' (1 - f) (1 - f_2)] . \quad (118)$$

Above,  $d\sigma_{NN}/d\Omega$  is the differential nucleon–nucleon cross–section and  $v_{12}$  is the relative velocity. In general, the mean field  $U$  depends on both the density  $n$  and the momentum  $\vec{p}$  of the nucleon. Equation (118) contains effects due to both hard collisions and soft interactions, albeit at a semiclassical level. Theoretical studies that confronted data have thus far used isospin averaged nucleon-nucleon cross sections and mean fields of symmetric nuclear matter. It is now well established that much of the collective behavior observed in experiments stems from momentum dependent forces at play during the early stages of the collision [84]. The conclusion that has emerged from several studies is that as long as momentum dependent forces are employed in models that analyze the data, a symmetric matter compression modulus of  $\sim 220$  MeV, as suggested by the analysis of the giant monopole resonance data [85], fits the heavy-ion data as well [86].

The prospects of rare isotope accelerators (RIA’s) that can collide highly neutron-rich nuclei has spurred further work to study a system of neutrons and protons at high neutron excess [87, 88, 89]. Generalizing Eq. (118) to a mixture, the kinetic equation for neutrons is

$$\frac{\partial f_n}{\partial t} + \vec{\nabla}_p U \cdot \vec{\nabla}_r f_n - \vec{\nabla}_r U \cdot \vec{\nabla}_p f_n = J_n = \sum_{i=n,p} J_{ni} , \quad (119)$$

where  $J_n$  describes collisions of a neutron with all other neutrons and protons. A similar equation can be written down for protons with appropriate modifications. On the left hand side of each coupled equation the mean field  $U \equiv U(n_n, n_p; \vec{p})$  depends explicitly on the neutron-proton asymmetry. The connection to the symmetry energy arises from the fact that  $U$  is obtained from a functional differentiation of a Hamiltonian density, such as that in Eq. (1). Examples of such mean fields may be found in Refs. [88, 89, 90]. Observables that are expected to shed light on the influence of isospin asymmetry include neutron-proton differential flow and the ratio of free neutron to proton multiplicity as a function of transverse momentum at midrapidity. Experimental investigations of these signatures await the development of RIA’s at GeV energies. In this connection, it will be important to detect neutrons in addition to protons.

## VI. DISCUSSION AND CONCLUSIONS

In this work, we have investigated the relationship between the symmetry energy of nucleonic matter and the neutron skin thicknesses of neutron-rich nuclei as well as the radii of neutron stars.

Precision measurements of neutron skins and neutron star radii are due to become available in the near future. We have studied how these measurements can constrain the dependence of the symmetry energy on baryon density,  $E_{sym}(n)$ , in the vicinity of the nuclear saturation density  $n_0$ . This knowledge is crucial to understanding many astrophysical phenomena, including neutron star evolution, supernova explosions and nucleosynthesis, and binary mergers involving neutron stars. Simulations of these phenomena involve extrapolations of the symmetry energy to supranuclear densities.

A crucial aspect of our presentation is that care was taken to ensure that the nuclear force parameterizations, whether for potential or field-theoretical models, were constrained by fits to closed-shell nuclei. In addition, all models were constrained to yield a maximum neutron star mass of at least  $1.44M_\odot$ , the larger of the accurately measured neutron star masses in the binary pulsar 1913+16. Without such constraints, much weaker correlations relating the neutron skin thickness to astrophysical quantities such as neutron star radii would have resulted.

Analytical representations of the relation between the symmetry energy and the neutron skin were developed for semi-infinite surfaces calculated in potential and field-theoretical models. To lowest order, the neutron skin thickness  $\delta R = \langle r_n^2 \rangle^{1/2} - \langle r_p^2 \rangle^{1/2}$  is proportional to  $\delta_L S_s / S_v$  where  $\delta_L$  is the neutron excess in the nuclear center and  $S_v [\equiv E_{sym}(n_0)]$  and  $S_s$  are related to the expansion parameters of the volume and surface symmetry energies, respectively, in the liquid drop or droplet models of nuclei. This representation is validated by comparisons with results of finite nucleus calculations performed in the Hartree-Fock-Bogoliubov (for potential models) and Hartree (for field-theoretical models) approximations. For the first time, results for nuclei are presented for the Akmal-Pandharipande-Ravenhall EOS parameterized according to both potential and field-theoretical models.

The semi-infinite surface representation predicts that the ratio  $S_s/S_v$ , or equivalently, the skin thickness  $\delta R$ , is a particular average of the density-dependent symmetry energy in the surface. In addition, phenomenological comparisons indicate that there is a relatively tight correlation between  $\delta R$  and the pressure of neutron star matter at a typical average surface density of  $5n_0/8$ . These results are not independent, but together imply that the determination of  $\delta R$  offers a valuable constraint on the density dependence of the symmetry energy. It was explicitly shown that the  $\delta R$  – pressure correlation is a consequence of a more general correlation between  $\delta R$  and the derivative of the symmetry energy at the same density. In contrast to most, but not all, previous results, we have also demonstrated that field theoretical models can yield a neutron skin thickness in  $^{208}\text{Pb}$  of less than 0.2 fm. Since a measurement of the neutron radius to about 1% accuracy implies an error of about 0.05 fm, the uncertainty in the neutron skin thickness will probably range from 10% to 30%, depending upon the magnitude of  $\delta R$ . On this basis, it is expected that the pressure at  $5/8 n_0$  could be determined to 20–50%.

An independent method of constraining  $S_s/S_v$  is from a least squares fit of nuclear models to nuclear binding energies. However, this fitting can only reliably establish a correlation between  $S_s/S_v$  and  $S_v$ . We have examined this in the liquid droplet approach using two plausible models. The surface tension was parameterized either in terms of  $\mu_n$ , implying a neutron skin, or in terms of  $\mu_n - \mu_p$  which allowed for the Coulomb interaction of protons. While these models gave fits to the data of similar accuracy, the valley in  $\chi^2$  differed in the two cases. The behavior of the ' $\mu_n$ ' model was shown to be more consistent with the systematic correlation derived from parameter optimization of both potential and field-theoretical models of laboratory nuclei.

The density dependence of the symmetry energy has a number of astrophysical consequences. One of the most important is its role in determining the composition of matter. In beta equilibrium, the proton fraction is proportional to  $E_{sym}(n)^3$  for small proton fractions. The charge fraction of matter plays an essential role in establishing the threshold densities of hyperons and the quark-hadron phase transition. If any of these threshold densities are exceeded in a neutron star, the

possibility of enhanced neutrino emission by a direct Urca process exists. The threshold for the direct Urca process involving nucleons alone is also determined by the charge fraction (for example, it is 1/9 in the absence of muons). We have shown that the determination of  $\delta R$  to have a value greater than approximately 0.2 fm would imply that at least the nucleon direct Urca process exists in  $1.4 M_{\odot}$  neutron stars.

An additional astrophysical application is the relation we established between  $\delta R$  and the radii  $R$  of neutron stars. Although Lattimer and Prakash established a phenomenological relation between  $R$  for a given mass star and the pressure of neutron star matter above, but near, the nuclear saturation density, there exists additional uncertainty in relating this algebraically to the  $\delta R - P$  correlation. However, as shown in this work, a useful relation directly relating  $\delta R$  and, for example, the radius of a  $1.4 M_{\odot}$  star,  $R_{1.4}$ , can be established.

The fact that the neutron skin thickness, which measures symmetry properties below nuclear density, and the astrophysical quantities involving the neutron star radius and the Urca threshold density, can be correlated is a consequence of a generic trend in the overall density dependence of the symmetry energy. This trend was specifically demonstrated by displaying the linear relationship which exists between the density derivatives of the symmetry energy at  $5n_0/8$  and  $3n_0/2$ . This relationship is independent of the parameterization of the nuclear force.

Observation of neutron star radii may provide qualitative information on the stellar composition. Using the parametric freedom of the EOS's considered, while satisfying the aforementioned constraints, we concluded that the minimum radius achievable for a star composed of just nucleons and leptons is about 9 km. Observation of a significantly smaller radius would likely imply that some softening component (bose condensates, hyperons, quarks, etc.) is present in dense matter, although it could also indicate that the EOS's given by potential and field-theoretical models is qualitatively incorrect.

We have also explored the influence of the density dependence of the nuclear symmetry energy on the transition pressure marking the boundary between the core and the crust in a neutron star. This transition pressure is closely approximated by the phase boundary separating uniform matter from matter in which nuclei exist. It was found that the transition pressure was not correlated with the neutron skin thickness, although the transition density did show some rather weak correlation. More interesting is the fraction of the star's moment of inertia residing in the crust which is measurable and which depends on the transition pressure, mass and radius. Here there was some correlation with larger values of this fraction tending to imply larger values of the neutron skin thickness, but the correlation was not very robust. Probably the neutron skin and the transition pressure should be viewed as independent quantities whose measurement would provide separate constraints on the EOS.

## ACKNOWLEDGMENTS

Research support of the U.S. Department of Energy under grant numbers DOE/DE-FG02-87ER-40328 (for AWS and PJE), and DOE/DE-FG02-87ER-40317 (for MP and JML) is acknowledged. We thank Chuck Horowitz and David Dean for providing us with computer codes for the calculation of the properties of finite nuclei.

## APPENDIX A: MODEL PROPERTIES

TABLE V: Saturation and surface properties for the models selected in this work. Symbols are  $n_0$ : nuclear matter saturation density in  $\text{fm}^{-3}$ ,  $B$ : the binding energy per particle in MeV,  $K$ : compression modulus in MeV,  $S_v$ : symmetry energy in MeV,  $S'_v$ : density derivative of the symmetry energy in  $\text{MeV fm}^3$ ,  $\sigma_0$ : surface tension of symmetric matter in  $\text{MeV fm}^{-2}$ ,  $\sigma_\delta$ : asymmetry parameter of the surface tension in  $\text{MeV fm}^{-2}$ , and  $\delta R$ : skin thickness of  $^{208}\text{Pb}$  in fm. The symbol “TW” in the second column refers to new models constructed in this work.

Model	Ref.	$n_0$	$B$	$K$	$S_v$	$n_0 S'_v$	$\sigma_0$	$\sigma_\delta$	$\delta R$
Potential									
Gs	[91]	0.15765	15.590	237.57	31.384	31.351	0.94198	6.4724	0.23730
Ly5	[TW]	0.16059	15.986	229.94	32.010	16.048	1.1469	3.8139	0.16600
Rs	[91]	0.15778	15.589	237.66	30.593	28.574	0.94257	5.8063	0.22240
SGI	[92]	0.15477	15.895	263.79	28.373	21.321	1.1156	4.0972	0.17650
SLy0	[93]	0.16030	15.973	229.67	31.982	15.704	1.1447	3.5963	0.16540
SLy230a	[94]	0.15998	15.990	229.89	31.985	14.772	1.1472	3.1525	0.15540
SkMP	[95]	0.15714	15.562	231.36	29.899	23.447	1.1063	5.1515	0.20030
SkT4	[39]	0.15902	15.957	235.56	35.457	31.380	0.98109	5.8878	0.25340
SkI5	[96]	0.15596	15.848	256.95	36.697	43.185	1.1492	7.7179	0.27540
NRAPR	[TW]	0.16058	15.856	225.70	32.787	19.880	1.0391	4.5347	0.19030
Field-theoretical									
NL4	[97]	0.14761	16.158	270.35	36.239	38.307	1.1706	6.2556	0.27346
S271	[7]	0.14840	16.250	271.00	35.927	24.240	0.95401	5.0735	0.25063
Z271	[7]	0.14840	16.250	271.00	35.369	22.334	0.89856	4.0940	0.23765
SR1	[TW]	0.16558	16.359	202.15	29.000	9.0730	1.0593	2.5161	0.15953
SR2	[TW]	0.15245	16.376	224.64	30.071	9.8437	0.95494	2.3783	0.17229
SR3	[TW]	0.15000	16.272	222.55	29.001	11.303	0.93076	2.4286	0.17096
es25	[TW]	0.16000	16.000	211.73	25.000	15.107	0.94625	2.4807	0.13769
es275	[TW]	0.16000	16.000	205.33	27.500	19.253	0.94558	3.2336	0.17135
es30	[TW]	0.16000	16.000	215.36	30.000	26.853	1.0281	4.7907	0.20542
es325	[TW]	0.16000	16.000	212.45	32.500	29.808	1.0232	5.3820	0.22536
es35	[TW]	0.15972	16.000	209.97	34.937	35.386	1.0369	6.4629	0.24843
RAPR	[TW]	0.15705	16.362	276.70	33.987	18.993	0.97931	3.1029	0.20114

**APPENDIX B: COUPLING STRENGTHS OF MODELS SR2, ES25, ES30, AND ES35**

TABLE VI: Coupling strengths for the model SR2 with nuclear matter equilibrium density  $n_0 = 0.15 \text{ fm}^{-3}$ , binding energy  $B = 16.38 \text{ MeV}$ , compression modulus  $K = 224.5 \text{ MeV}$ , Dirac effective mass  $M^*(n_0) = 0.78M$ , and symmetry energy  $E_{sym} = 30.1 \text{ MeV}$ . The dimensions of  $a_i$  and  $b_i$  are such that the Lagrangian in Eq. (13) is in  $\text{MeV}^4$ .

$m_\sigma$	$g_\sigma$	$g_\omega$	$g_\rho$	$\kappa$	$\lambda$
440.93 MeV	7.1513	8.9644	11.217	14.055 MeV	0.010091
$\zeta$	$\xi$	$a_1$	$a_2$	$a_3$	$a_4$
0.052964	3.0351	35.470	$5.0570 \times 10^{-3}$	$2.3109 \times 10^{-6}$	$1.0686 \times 10^{-3}$
$a_5$	$a_6$	$b_1$	$b_2$	$b_3$	
$1.0060 \times 10^{-11}$	$6.8908 \times 10^{-7}$	0.22299	$2.2908 \times 10^{-7}$	$3.0076 \times 10^{-13}$	

TABLE VII: Coupling strengths for the model es25 with nuclear matter equilibrium density  $n_0 = 0.16 \text{ fm}^{-3}$ , binding energy  $B = 16 \text{ MeV}$ , compression modulus  $K = 211.7 \text{ MeV}$ , Dirac effective mass  $M^*(n_0) = 0.76M$ , and symmetry energy  $E_{sym} = 25 \text{ MeV}$ . For the couplings  $a_i$  and  $b_i$ , only the non-zero entries are given.

$m_\sigma$	$g_\sigma$	$g_\omega$	$g_\rho$	$\kappa$	$\lambda$
459.52 MeV	7.5425	9.1120	8.3802	16.504 MeV	-0.052591
$\zeta$	$\xi$	$a_2$	$b_1$		
$1.5174 \times 10^{-3}$	0.12740	3.4477	1.5931		

TABLE VIII: Coupling strengths for the model es30 with nuclear matter equilibrium density  $n_0 = 0.16 \text{ fm}^{-3}$ , binding energy  $B = 16 \text{ MeV}$ , compression modulus  $K = 215.4 \text{ MeV}$ , Dirac effective mass  $M^*(n_0) = 0.66M$ , and symmetry energy  $E_{sym} = 30 \text{ MeV}$ . Only non-zero  $a_i$  and  $b_i$  are given.

$m_\sigma$	$g_\sigma$	$g_\omega$	$g_\rho$	$\kappa$	$\lambda$
503.18 MeV	9.2236	11.173	7.5106	7.3353 MeV	-0.028115
$\zeta$	$\xi$	$a_2$	$b_1$		
$2.9571 \times 10^{-3}$	0.20174	0.57839	0.22445		

TABLE IX: Coupling strengths for the model es35 with nuclear matter equilibrium density  $n_0 = 0.1597 \text{ fm}^{-3}$ , binding energy  $B = 16 \text{ MeV}$ , compression modulus  $K = 210.0 \text{ MeV}$ , Dirac effective mass  $M^*(n_0) = 0.64M$ , and symmetry energy  $E_{sym} = 34.93 \text{ MeV}$ . Only non-zero  $a_i$  and  $b_i$  are given.

$m_\sigma$	$g_\sigma$	$g_\omega$	$g_\rho$	$\kappa$	$\lambda$
508.88 MeV	9.5598	11.576	8.1475	6.6428 MeV	-0.028032
$\zeta$	$\xi$	$a_2$	$b_1$		
$-5.8216 \times 10^{-5}$	0.067440	0.024880	0.014600		

---

[1] J. M. Lattimer and M. Prakash, Phys. Rep. **333**, 121 (2000).

[2] J. M. Lattimer and M. Prakash, Astrophys. J. **550**, 426 (2001).

[3] B. A. Brown, Phys. Rev. Lett **85**, 5296 (2000).

[4] S. Typel and B. A. Brown, Phys. Rev. C **64**, 027302 (2001).

[5] H. Krivine, Jour. de Phys. Supp. **C6**, 153 (1984).

[6] J. M. Lattimer, in *Nuclear Equation of State*, edited by A. Ansari and L. Satpathy (World Scientific, Singapore, 1996), p. 83.

[7] C. J. Horowitz and J. Piekarewicz, Phys. Rev. Lett. **86**, 5647 (2001).

[8] C. J. Horowitz, S. J. Pollock, P. A. Souder, and R. Michaels, Phys. Rev. C **63**, 025501 (2001).

[9] R. Michaels, P. A. Souder, and G. M. Urciuoli, Jefferson Laboratory Proposal **PR-00-003** (2000).

[10] B. C. Clark, L. J. Kerr, and S. Hama, Phys. Rev. C **67**, 054605 (2003).

[11] A. Trzcińska, J. Jastrzębski, P. Lubiński, F. J. Hartmann, R. Schmidt, T. von Egidy, and B. Kłos, Phys. Rev. Lett **87**, 082501 (2001).

[12] S. Karataglidis, K. Amos, B. A. Brown, and P. K. Deb, Phys. Rev. C **65**, 044306 (2002).

[13] A. Akmal, V. R. Pandharipande, and D. G. Ravenhall, Phys. Rev. C **58**, 1804 (1998).

[14] A. Akmal and V. R. Pandharipande, Phys. Rev. C **56**, 2261 (1997).

[15] B. D. Serot and J. D. Walecka, in *Adv. Nucl. Phys.*, edited by J. W. Negele and E. Vogt (Plenum, 1989), vol. 16, p. 1.

[16] P. Hohenberg and W. Kohn, Phys. Rev. **136**, B864 (1964).

[17] W. Kohn and L. J. Sham, Phys. Rev. **140**, A1133 (1965).

[18] S. C. Pieper and R. B. Wiringa, Ann. Rev. Nucl. Part. Sci. **51**, 53 (2001).

[19] T. H. R. Skyrme, Nucl. Phys. **9**, 615 (1959).

[20] D. Vautherin and D. M. Brink, Phys. Rev. C **5**, 626 (1972).

[21] P.-G. Reinhard, D. J. Dean, W. Nazarewicz, J. Dobaczewski, J. A. Maruhn, and M. R. Strayer, Phys. Rev. C **60**, 014316 (1999).

[22] J. P. Blaizot, Phys. Rep. **64**, 171 (1980).

[23] M. Prakash, T. L. Ainsworth, and J. M. Lattimer, Phys. Rev. Lett **61**, 2518 (1988).

[24] H. Müller and B. D. Serot, Nucl. Phys. A **606**, 508 (1996).

[25] C. J. Pethick, D. G. Ravenhall, and C. P. Lorenz, Nucl. Phys. A **584**, 675 (1995).

[26] J. Boguta and A. R. Bodmer, Nucl. Phys. A **292**, 413 (1977).

[27] W. Stocker and M. M. Sharma, Z. Phys. A **339**, 147 (1991).

[28] J. M. Lattimer, C. J. Pethick, D. G. Ravenhall, and D. Q. Lamb, Nucl. Phys. A **432**, 646 (1985).

[29] W. D. Myers and W. J. Swiatecki, Ann. Phys. **55**, 395 (1969).

[30] H. Krivine and J. Treiner, Phys. Lett. B **124**, 127 (1983).

[31] E. Lipparini and S. Stringari, Phys. Lett. B **112**, 421 (1982).

[32] J. Treiner and H. Krivine, Ann. Phys. **170**, 406 (1986).

[33] P. Danielewicz, Nucl. Phys. A **727**, 233 (2003).

[34] C. J. Horowitz and B. D. Serot, Nucl. Phys. A **368**, 503 (1981).

[35] B. Frois and C. N. Papanicolas, Ann. Rev. Nucl. Part. Sci. **37**, 133 (1987).

[36] B. G. Todd and J. Piekarewicz, Phys. Rev. C **67**, 044317 (2003).

[37] J. M. Lattimer and M. Prakash, Science **304**, 536 (2004).

[38] J. Dobaczewski, H. Flocard, and J. Treiner, Nucl. Phys. A **422**, 103 (1984).

[39] F. Tondeur, M. Brack, M. Farine, and J. M. Pearson, Nucl. Phys. A **420**, 297 (1984).

[40] J. R. Stone, J. C. Miller, R. Konciewicz, P. D. Stevenson, and M. R. Strayer, Phys. Rev. C **68**, 034324 (2003).

[41] J. Margueron, J. Navarro, and N. Van Giai, Phys. Rev. C **66**, 014303 (2002).

[42] C. J. Batty, E. Friedman, H. J. Gils, and H. Rebel, in *Adv. Nucl. Phys.*, edited by J. W. Negele and E. Vogt (Plenum, 1989), vol. 19, p. 1.

[43] G. Fricke, C. Bernhardt, K. Heilig, L. A. Schaller, L. Schellenberg, E. B. Shera, and C. W. de Jager, At. Data Nucl. Data Tables **60**, 177 (1995).

[44] G. Audi, A. H. Wapstra, and C. Thibault, Nucl. Phys. A **729**, 337 (2003).

[45] V. E. Starodubsky and N. M. Hintz, Phys. Rev. C **49**, 2118 (1994).

[46] L. Ray, G. W. Hoffmann, G. S. Blanpied, W. R. Coker, and R. P. Liljestrand, Phys. Rev. C **18**, 1756

(1978).

[47] W. R. Gibbs and J.-P. Dedonder, Phys. Rev. C **46**, 1825 (1992).

[48] H. de Vries, C. W. de Jager, and C. de Vries, At. Data Nucl. Data Tables **36**, 495 (1987).

[49] P. Møller, J. R. Nix, W. D. Myers, and W. J. Swiatecki, At. Data and Nucl. Data Tables **59**, 185 (1995).

[50] J. M. Lattimer and F. D. Swesty, Nucl. Phys. A **535**, 331 (1991).

[51] A. Burrows and J. Lattimer, Astrophys. J. **285**, 294 (1984).

[52] A. R. Bodmer and Q. R. Usmani, Phys. Rev. C **67**, 034305 (2003).

[53] A. R. Bodmer, Nucl. Phys. **17**, 388 (1960).

[54] R. J. Furnstahl, Nucl. Phys. A **706**, 85 (2002).

[55] M. Prakash, in *Nuclear Equation of State*, edited by A. Ansari and L. Satpathy (World Scientific, Singapore, 1996), p. 229.

[56] M. Baldo, C. Maieron, P. Schuck, and X. Viñas, Nucl. Phys. A **736**, 241 (2004).

[57] E. Flowers, M. Ruderman, and P. Sutherland, Astrophys. J. **205**, 541 (1976).

[58] C. J. Horowitz and J. Piekarewicz, Phys. Rev. C **66**, 055803 (2002).

[59] D. Page, J. M. Lattimer, M. Prakash, and A. W. Steiner, astro-ph/0403657 (2004).

[60] B. Link, R. I. Epstein, and J. M. Lattimer, Phys. Rev. Lett. **83**, 3362 (1999).

[61] D. Q. Lamb, J. M. Lattimer, and D. G. Pethick, C. J. and Ravenhall, Nucl. Phys. A **411**, 449 (1983).

[62] H. A. Buchdahl, Astrophys. J. **147**, 310 (1967).

[63] S. Schramm, Phys. Lett. B **560**, 164 (2003).

[64] C. J. Horowitz and J. Piekarewicz, Phys. Rev. C **64**, 062802(R) (2001).

[65] E. Lipparini and S. Stringari, Phys. Rep. **103**, 175 (1989).

[66] R. Bergère, in *Lecture Notes in Physics*, edited by S. Costa and C. Schaefer (Springer-Verlag, 1977), vol. 61, p. 1.

[67] R. M. Laszewski and P. Axel, Phys. Rev. C **19**, 342 (1979).

[68] O. Bohigas, N. Van Giai, and D. Vautherin, Phys. Lett. B **102**, 105 (1981).

[69] H. Krivine, C. Schmit, and J. Treiner, Phys. Lett. B **112**, 281 (1983).

[70] E. Lipparini and S. Stringari, Nucl. Phys. A **482**, 205c (1988).

[71] S. Khamerdzhiev, J. Speth, and G. Tertychny, Nucl. Phys. A **624**, 328 (1997).

[72] P. Chomaz, M. Colonna, and J. Randrup, Phys. Rep. **389**, 263 (2004).

[73] B. A. Li and C. M. Ko, Nucl. Phys. A **618**, 498 (1997).

[74] H. S. Xu, M. B. Tsang, T. X. Liu, X. D. Liu, W. G. Lynch, W. P. Tan, A. Vander Molen, G. Verde, A. Wagner, H. F. Xi, et al., Phys. Rev. Lett. **85**, 716 (2000).

[75] M. B. Tsang, W. A. Friedman, C. K. Gelbke, W. G. Lynch, G. Verde, and H. S. Xu, Phys. Rev. Lett. **86**, 5023 (2001).

[76] A. Ono, P. Danielewicz, W. A. Friedman, W. G. Lynch, and M. B. Tsang, Phys. Rev. C **68**, 051601(R) (2003).

[77] C. B. Das, S. Das Gupta, W. G. Lynch, A. Z. Mekjian, and M. B. Tsang, Phys. Rep. **Submitted** (2004).

[78] H. H. Gutbrod, A. M. Poskanzer, and H. G. Ritter, Rep. Prog. Phys. **52**, 267 (1989).

[79] P. Danielewicz and G. Odyniec, Phys. Lett. B **157**, 146 (1985).

[80] H. A. Gustafsson, H. H. Gutbrod, B. Kolb, H. Löhner, B. Ludewigt, A. M. Poskanzer, T. Renner, H. Riedesel, H. G. Ritter, A. Warwick, et al., Phys. Rev. Lett. **52**, 1590 (1984).

[81] G. M. Welke, M. Prakash, T. T. S. Kuo, S. Das Gupta, and C. Gale, Phys. Rev. C **38**, 2101 (1988).

[82] P. Siemens and J. O. Rasmussen, Phys. Rev. Lett. **42**, 880 (1979).

[83] G. F. Bertsch and S. Das Gupta, Phys. Rep. **160**, 189 (1988).

[84] C. Gale, G. M. Welke, M. Prakash, S. J. Lee, and S. Das Gupta, Phys. Rev. C **41**, 1545 (1990).

[85] D. H. Youngblood, H. L. Clark, and Y.-W. Lui, Phys. Rev. Lett. **82**, 691 (1999).

[86] P. Danielewicz, R. Lacey, and W. G. Lynch, Science **298**, 1592 (2002).

[87] C. B. Das, S. Das Gupta, C. Gale, and B.-A. Li, Phys. Rev. C **67**, 034611 (2003).

[88] B.-A. Li, C. B. Das, S. Das Gupta, and C. Gale, Phys. Rev. C **88**, 192701 (2004).

[89] B.-A. Li, C. B. Das, S. Das Gupta, and C. Gale, Nucl. Phys. A **735**, 563 (2004).

[90] M. Prakash, I. Bombaci, M. Prakash, P. J. Ellis, and J. M. Lattimer, Phys. Rep. **280**, 1 (1997).

[91] J. Friedrich and P.-G. Reinhard, Phys. Rev. C **33**, 335 (1986).

[92] N. Van Giai and H. Sagawa, Phys. Lett. B **106**, 379 (1981).

- [93] E. Chabanat, thesis (unpublished) (1995).
- [94] E. Chabanat, P. Bonche, P. Haensel, J. Meyer, and R. Schaeffer, Nucl. Phys. **A627**, 710 (1997).
- [95] L. Bennour, P.-H. Heenen, P. Bonche, J. Dobaczewski, and H. Flocard, Phys. Rev. C **40**, 2834 (1989).
- [96] P.-G. Reinhard and H. Flocard, Nucl. Phys. A **584**, 467 (1995).
- [97] B. Nerlo-Pomorska and J. Sykut, Int. J. Mod. Phys. E **13**, 75 (2004).